



# Seasonal and spatial variations of greenhouse gas (CO<sub>2</sub>, CH<sub>4</sub> and N<sub>2</sub>O) emissions from urban ponds in Brussels

T. Bauduin<sup>a,b,\*</sup>, N. Gypens<sup>a</sup>, A.V. Borges<sup>b</sup>

<sup>a</sup> Ecology of Aquatic Systems, Free University of Brussels, Belgium

<sup>b</sup> Chemical Oceanography Unit, University of Liège, Belgium

## ARTICLE INFO

### Keywords:

Carbon dioxide  
Methane  
Nitrous oxide  
Brussels  
Urban ponds  
Urban ecology  
Macrophytes

## ABSTRACT

Freshwaters have been recognized as important sources of greenhouse gases (GHG) to the atmosphere. However, urban ponds have received little attention even though their number is increasing due to expanding urbanisation globally. Ponds are frequently associated to urban green spaces that provide several ecosystemic services such as cooling local climate, regulating the water cycle, and acting as small carbon sinks. This study aims to identify and understand the processes producing GHGs (CO<sub>2</sub>, CH<sub>4</sub>, and N<sub>2</sub>O) in the urban ponds of the temperate European city of Brussels in Belgium. 22 relatively small ponds (0.1–4.6 ha) surrounded by contrasted landscape (strictly urban, bordered by cropland or by forest), were sampled during four seasons in 2021–2022. The mean ± standard deviation was 3,667 ± 2,904 ppm for the partial pressure of CO<sub>2</sub> (pCO<sub>2</sub>), 2,833 ± 4,178 nmol L<sup>-1</sup> for CH<sub>4</sub>, and 273 ± 662% for N<sub>2</sub>O saturation level (%N<sub>2</sub>O). Relationships of GHGs with oxygen and water temperature suggest that biological processes controlled pCO<sub>2</sub>, CH<sub>4</sub> concentration and %N<sub>2</sub>O. However, pCO<sub>2</sub> was also controlled by external inputs as indicated by the higher values of pCO<sub>2</sub> in the smaller ponds, more subject to external inputs than larger ones. The opposite was observed for CH<sub>4</sub> concentration that was higher in larger ponds, closer to the forest in the city periphery, and with higher macrophyte cover. N<sub>2</sub>O concentrations, as well as dissolved inorganic nitrogen, were higher closer to the city center, where atmospheric nitrogen deposition was potentially higher. The total GHG emissions from the Brussels ponds were estimated to 1kt CO<sub>2</sub>-eq per year and were equivalent to the carbon sink of urban green spaces.

## 1. Introduction

The three main greenhouse gases (GHGs) emitted to the atmosphere by human activities are carbon dioxide (CO<sub>2</sub>), methane (CH<sub>4</sub>) with a global warming potential (GWP) 34 times greater than CO<sub>2</sub> on a 100-year time scale, and nitrous oxide (N<sub>2</sub>O) with a GWP 298 times greater than CO<sub>2</sub> on a 100-year time scale (Myrhe et al., 2013). In inland waters, the production of CO<sub>2</sub> and CH<sub>4</sub> are mainly due to the degradation of organic matter (OM) through mainly aerobic processes for CO<sub>2</sub> (Del Giorgio et al., 1999; Cole and Caraco, 2001) and by anaerobic archaeal methanogenesis for CH<sub>4</sub> (Conrad, 2020). The OM in inland waters can be autochthonous or allochthonous. Autochthonous production of OM is from phytoplankton (McClure et al., 2020; Bartosiewicz et al., 2021) or aquatic macrophytes (Grasset et al., 2019; Desrosiers et al., 2022). The relation between autochthonous biomass (phytoplankton and macrophytes) and CH<sub>4</sub> emissions is well established (DelSontro et al., 2018; Borges et al., 2022; Bastviken et al., 2023). The

impact of autochthonous biomass on CO<sub>2</sub> depends on the phase of the bloom development, high concentrations of chlorophyll-*a* (Chl-*a*) during the growth and peak phases coinciding with intense photosynthesis and CO<sub>2</sub> consumption (Grasset et al., 2020; Borges et al., 2022), and phases of senescence leading to CO<sub>2</sub> production. Allochthonous OM in small water bodies (e.g., ponds) comes from fallen leaves of the surrounding vegetation and from particulate and dissolved OM from surface runoff or from soil-water and groundwater inputs (Gasith and Hosier, 1976; Weyhenmeyer et al., 2015). The N<sub>2</sub>O production is mainly due to microbial nitrification and denitrification and is dependent on the availability of dissolved inorganic nitrogen (DIN) and O<sub>2</sub> (Codispoti and Christensen, 1985; Mengis et al., 1997). Anthropogenic nitrogen inputs from leakage of fertilizers from croplands or from atmospheric deposition may enhance the N<sub>2</sub>O emissions in freshwater wetlands, lakes and rivers (McCrackin and Elser, 2011; Bettez and Goffman, 2013; Sønderup et al., 2016; D'Acunha and Johnson, 2019; Decina et al., 2020; Bonetti et al., 2022).

\* Corresponding author at: Ecology of Aquatic Systems, Free University of Brussels, Belgium.

E-mail address: [thomas.bauduin@ulb.be](mailto:thomas.bauduin@ulb.be) (T. Bauduin).

<https://doi.org/10.1016/j.watres.2024.121257>

Received 10 August 2023; Received in revised form 23 January 2024; Accepted 1 February 2024

Available online 2 February 2024

0043-1354/© 2024 Elsevier Ltd. All rights reserved.

The emissions from inland waters (rivers-streams, lakes and reservoirs) of GHGs were estimated at  $14.3 \text{ Pg CO}_2 \text{ yr}^{-1}$  for  $\text{CO}_2$  (Drake et al., 2018),  $6.03 \text{ Pg CO}_2 \text{ equivalent (CO}_2\text{-q) yr}^{-1}$  for  $\text{CH}_4$  (Rosentreter et al., 2021) and  $0.05 \text{ Pg CO}_2\text{-eq yr}^{-1}$  for  $\text{N}_2\text{O}$  (Lauerwald et al., 2019). Yet, these estimates remain highly uncertain because of the low number of measurements that is insufficient to account for the strong spatial and temporal variability of the fluxes within a given system, as well as the high diversity of systems due to differences in size, climate, catchment morphology, land cover, and anthropogenic pressures.

Several studies have shown the importance of small water bodies (surface area  $< 0.1 \text{ ha}$ ) as hotspots for GHG emissions (Holgerson and Raymond, 2016; Grinham et al., 2018; Rosentreter et al., 2021; Peacock et al., 2021). Although only representing 9 % of the total area of lentic waters, small water bodies account for 15 % and 40 % of diffusive emissions from lakes of  $\text{CO}_2$  and  $\text{CH}_4$ , respectively according to Holgerson and Raymond (2016). Urban areas have a large number of small water bodies in the form of ponds mostly associated to green spaces such as public parks, and their number is increasing due to rapid urbanisation worldwide (Brans et al., 2018; Audet et al., 2020). Yet, only a very limited number of studies have investigated GHG emissions from urban ponds (Singh et al., 2000; Natchimuthu et al., 2014; van Bergen et al., 2019; Audet et al., 2020; Peacock et al., 2021). Urban ponds are small

and thus have high ratio of perimeter to surface area (Hanson et al., 2007), surrounded by impervious surfaces (Davidson et al., 2015; Peacock et al., 2021), and a high stormwater runoff that combined result in high inputs of OM and DIN that should sustain emissions of  $\text{CO}_2$ ,  $\text{CH}_4$ , and  $\text{N}_2\text{O}$  to the atmosphere. Additionally, urban ponds are usually very shallow so there is a strong influence on the water column of GHG production in sediments.

Brussels is the most densely populated area in Belgium and the largest city of the country and contains 158 ponds totalling a surface area of 101 ha. The population is more than 1 million inhabitants, equating to less than  $1 \text{ m}^2$  of water body per inhabitant, indicating a high degree of anthropogenic pressure on these ecosystems. However, not all urban ponds are subject to the same degree of anthropogenic pressure, as the periphery of the city is bordered by cropland and forest. Yet, the ponds in Brussels are highly eutrophied with in some cases high algal biomass but also macrophytes which compete with phytoplankton for nutrients (Peretyatko et al., 2007; de Backer et al., 2010, 2012; Descy et al., 2016). Yet, the equilibrium between the prevalence of macrophytes and phytoplankton entails a gradual shift rather than an abrupt process and is influenced by additional factors other than nutrient levels (Van Nes et al., 2002; Davidson et al., 2023). It can be hypothesized that water bodies with a dominance of phytoplankton and a dominance of

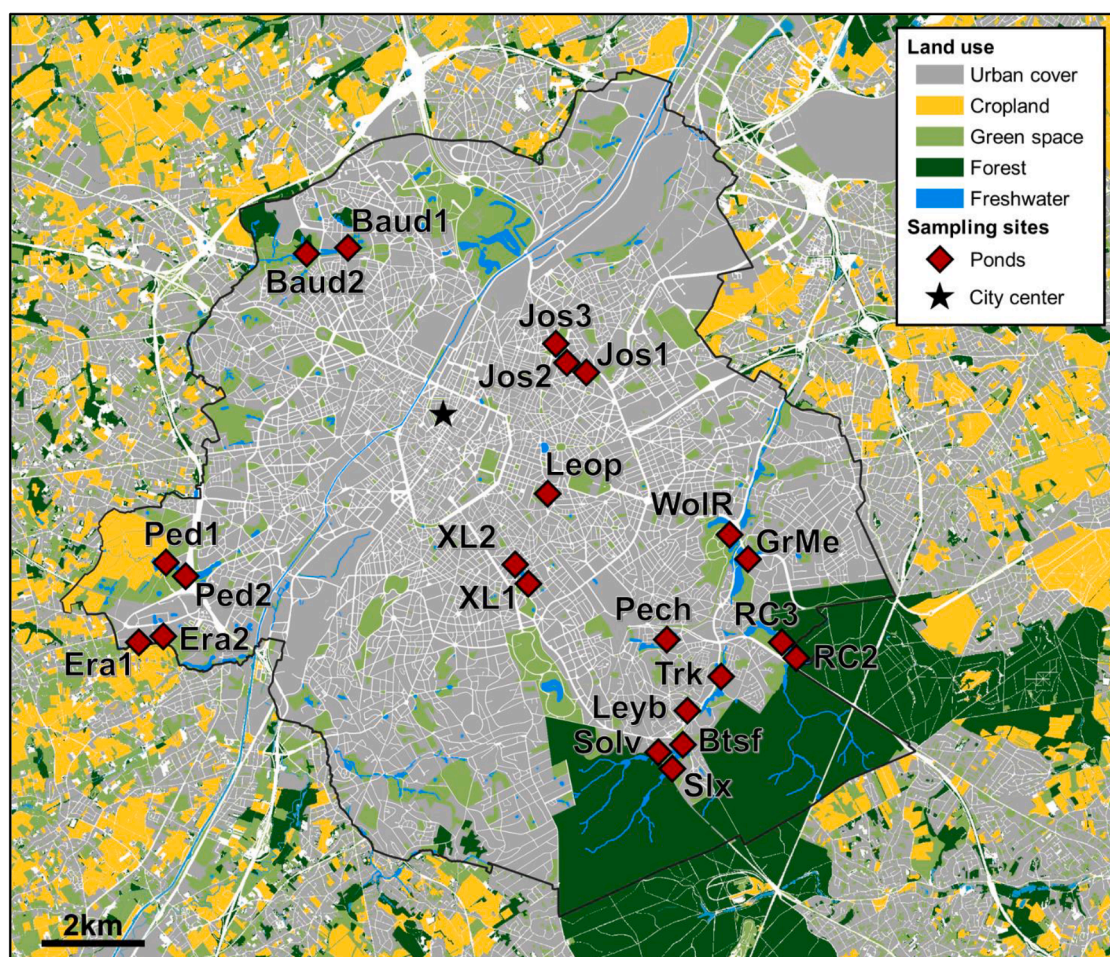


**Fig. 1.** Map of the metropolitan area of the region of Brussels delineated by the black line and surrounding region of Flanders in Belgium showing land cover and sampling locations in ponds (red diamonds). The star corresponds to the center of the city ( $50.8504^\circ \text{N}$ ,  $4.3487^\circ \text{E}$ ). The acronyms correspond to the official names of the ponds of Bruxelles Environnement, the regional water management agency (Baud 1: Etang Parc Roi Baudouin Phase I; Baud2: Etang Parc Roi Baudouin Phase II; Btsf: Etang de Boitsfort; Era 1: Etang Erasme amont; Era 2: Etang Erasme aval; GrMe: Grand étang Mellaerts; Jos1: Parc Josaphat - Etang aux canards; Jos2: Parc Josaphat - Etang aux pigeons; Jos3: Parc Josaphat - Etang de la laiterie; Leop: Etang parc Leopold; Leyb: Etang du Leybeek; Pech: Etang Pêcheries Royales; Ped1: Etang de la Pède Grand Etang; Ped2: Etang de la Pède; RC2: Grand étang des Clabots (Etang 2); RC3: Etang du moulin (Etang 3); Slx: Etang du Silex; Solv: Grand étang - Parc Tournay Solvay; Trk: Etang Parc Ten Reuken; WolR: Etang rond - Parc de Woluwe; XL1: Etang d'Ixelles Nord; XL2: Etang d'Ixelles Sud). The shape of each pond and connection to the hydrological network is shown in Fig. S1.

macrophytes should have different GHG dynamics, although this has seldom been tested (Harpenslager et al., 2022; Balaña et al., 2023).

Here, we report CO<sub>2</sub>, CH<sub>4</sub>, and N<sub>2</sub>O dissolved concentrations and complementary variables (water temperature, chlorophyll-*a* (Chl-*a*), DIN, and O<sub>2</sub>) sampled in 22 small urban ponds (0.1–4.6 ha) of the city of Brussels, during the four seasons in 2021–2022. Potential drivers of CO<sub>2</sub>, CH<sub>4</sub>, and N<sub>2</sub>O dynamics are investigated by comparing pond size, presence of macrophytes, relative distance to the city center, surrounding landscape (strictly urban, bordered by cropland or by forest). We test if the most frequent accepted hypotheses of the drivers of CO<sub>2</sub>, CH<sub>4</sub> and N<sub>2</sub>O seasonal and spatial variations in natural lakes and ponds also apply to urban ponds. The CO<sub>2</sub>, CH<sub>4</sub>, and N<sub>2</sub>O diffusive emissions are computed and compared to the official inventory of GHG emissions from the city of Brussels.

## 2. Material and methods

### 2.1. Pond selection and sampling frequency

22 ponds were selected within the Brussels region (Fig. 1). All of the ponds are artificial and were built during the past century, the majority with the primary aim of landscaping and embellishing parks. Recreational fishing activities are allowed in four of the sampled ponds (Table S1). Some of the sampled ponds are connected to a river network (flow-through ponds) and others are fed directly by groundwater and small watercourses (overflow ponds), where water level is kept constant by an overflow outlet (Table S1). The sampled ponds are in the four main catchment areas of the city of Brussels (Molenbeek (*n* = 2), Neerpedebeek-Vogelzangbeek (*n* = 4), Maelbeek (*n* = 6), and Woluwe (*n* = 10) catchments) (Table S1). Four sampling campaigns were carried out on the 22 ponds, corresponding to the four seasons: November 2021 (Fall), February 2022 (Winter), May 2022 (Spring) and August 2022 (Summer).

### 2.2. Meteorological data

Air temperature, rainfall and wind speed were retrieved from <http://www.meteo.be/fr> for the meteorological station of the Royal Meteorological Institute of St-Lambert (50.8408 °N, 4.4234 °E) in Brussels, located between 1 and 10 km from the sampled ponds. Wind speeds and air temperatures were averaged over 24 h to obtain a daily average value. The rainfall was integrated on each day to obtain the daily rainfall.

### 2.3. Sampling in field

Water was sampled and collected from pontoons. Water pH, temperature, conductivity and oxygen saturation level (%O<sub>2</sub>) were measured by a VWR MU 6100 H probe. Water was collected in 2 L polypropylene bottles for subsequent sampling for Chl-*a*, total suspended matter (TSM) and dissolved inorganic nutrients (ammonium (NH<sub>4</sub><sup>+</sup>), nitrite (NO<sub>2</sub><sup>-</sup>), nitrate (NO<sub>3</sub><sup>-</sup>), soluble reactive phosphorus (SRP)). Three 50 mL falcon tubes were filled with unfiltered water to which was added 200 μL of HNO<sub>3</sub> (65 %) for total phosphorus (P<sub>tot</sub>) analysis.

Macrophytes were defined as vascular aquatic plants, excluding filamentous algae, mosses and liverworts, (Bowden et al., 2017). The percentage of macrophyte cover was estimated visually during sampling. Dominant species of macrophytes (*Potamogeton pectinatus*, *Ceratophyllum demersum*, *Chara* sp., *Nitella* sp., *Lemna trisulca*, *Zannichellia palustris*) were identified in August 2022, when macrophyte cover was maximal. This list of species of macrophytes agreed with past studies in Brussels ponds (Peretyatko et al., 2010; de Backer et al., 2010).

### 2.4. Laboratory analysis

Water was filtered on Whatman filters 0.7 μm GF/F glass microfibers

with diameter of 47 mm for TSM and Chl-*a* (stored frozen). Filtered water was stored in 50 ml plastic vials and stored frozen for dissolved nutrients analysis. Chl-*a* was measured on extracts with 90 % acetone by fluorimetry (Kontron SFM 25 model) (Yentsch and Menzel, 1963). NH<sub>4</sub><sup>+</sup> was determined with the nitroprusside-hypochlorite-phenol coloration method (Grasshoff and Johannsen, 1972). NO<sub>2</sub><sup>-</sup> and NO<sub>3</sub><sup>-</sup> were determined before and after reduction of NO<sub>3</sub><sup>-</sup> to NO<sub>2</sub><sup>-</sup> by a cadmium-copper column, with Griess' reagent in acidic medium coloration method (Grasshoff and Kremling, 2009). SRP was determined with ammonium molybdate, ascorbic acid and potassium antimony tartrate coloration method (Koroleff, 1983).

P<sub>tot</sub> was determined by inductively coupled plasma spectroscopy (ICP) on an ICP-OES Perkin Elmer Avio 200 model. The assay protocol was based on the US EPA (1994) method 200.7 for analysis of metals and trace elements in water by ICP with prior microwave acid digestion based on US EPA (2007) method 3015A.

### 2.5. Measurement of GHG concentrations and computation of fluxes

CO<sub>2</sub> measurements were carried out on the field with a Li-Cor Li-840 CO<sub>2</sub>/H<sub>2</sub>O gas analyser using the headspace technique with 4 polypropylene syringes of 60 mL. The technique consisted in equilibrating inside the syringe 30 mL of sample water with 30 mL of atmospheric air by vigorous shaking during 5 min. The headspace of each syringe was injected sequentially in the Li-840 and a fifth syringe was used to measure atmospheric CO<sub>2</sub>. The final pCO<sub>2</sub> value was computed taking into account the partitioning of CO<sub>2</sub> between water and the headspace, as well as equilibrium with HCO<sub>3</sub><sup>-</sup> (Dickson et al., 2007) using water temperature measured in-stream and after equilibration, and total alkalinity (data not shown). Samples for total alkalinity were conditioned, stored and analysed as described by Borges et al. (2019). The Li-Cor Li-840 was calibrated before and after each sampling period with ultrapure N<sub>2</sub> and a suite of gas standards (Air Liquide Belgium) with CO<sub>2</sub> mixing ratios of 388, 813, 3788 and 8300 ppm. The overall precision of pCO<sub>2</sub> measurements was ±2 %.

Samples for dissolved CH<sub>4</sub> and N<sub>2</sub>O were collected directly in surface waters with 60 ml plastic syringes and transferred with a plastic tube into two 60 mL borosilicate serum bottles and poisoned with 200 μL of saturated HgCl<sub>2</sub> solution. The vials were sealed with a butyl stopper and crimped with an aluminium cap. Measurements were carried out using the headspace technique with a SRI 8610C gas chromatograph with a flame ionisation detector (FID) for CH<sub>4</sub> and an electron capture detector (ECD) for N<sub>2</sub>O, calibrated with CH<sub>4</sub>:N<sub>2</sub>O:N<sub>2</sub> gas mixtures (Air Liquide Belgium) with mixing ratios of 1, 10, 30, 509, and 2010 ppm for CH<sub>4</sub>, and 0.2, 2.0 and 6.0 ppm for N<sub>2</sub>O. The precision of measurement was ±11 % for CH<sub>4</sub> and ±6 % for N<sub>2</sub>O based on 176 replicates. Ebullitive CH<sub>4</sub> fluxes were not measured during this study, but were measured with inverted funnels (e.g. Keller and Stallard 1994) in four ponds (Leybeek, Pêcheres Royales, Silex, Ten Reuken) for the period of 29/03/22 to 09/09/23 (unpublished data).

The CO<sub>2</sub> concentration is expressed in terms of partial pressure of CO<sub>2</sub> (pCO<sub>2</sub> in ppm), the CH<sub>4</sub> dissolved concentration in nmol L<sup>-1</sup> corresponding to the usual convention in topical literature. N<sub>2</sub>O concentrations oscillated around atmospheric equilibrium, so the data are presented as a percentage of the saturation level (%N<sub>2</sub>O), where 100 % corresponds to atmospheric equilibrium. The atmospheric pCO<sub>2</sub> was measured on the field with the Li-Cor Li-840. The equilibrium with atmosphere for N<sub>2</sub>O was calculated from the average air mixing ratios of N<sub>2</sub>O provided by the Global Monitoring Division (GMD) of the National Oceanic and Atmospheric Administration (NOAA) Earth System Research Laboratory (ESRL) (Dutton et al., 2017). A constant atmospheric concentration of 1.9 ppm was assumed for CH<sub>4</sub>.

The exchange of CO<sub>2</sub>, CH<sub>4</sub>, and N<sub>2</sub>O between surface water and the atmosphere was calculated according to:

$$F_G = k_g \Delta C$$

$F_G$  ( $\text{mmol m}^{-2}\text{d}^{-1}$ ) is the flux of a specific gas (G),  $k_g$  ( $\text{cm h}^{-1}$ ) is the specific gas transfer velocity, and  $\Delta C$  is the gas concentration gradient in water and the atmosphere ( $\text{mmol L}^{-1}$ ).

The  $k_g$  values were derived from the gas transfer velocity normalized to Schmidt number of 600 ( $k_{600}$ ) according to:

$$k_g = k_{600} \times (Sc/600)^{-0.5}$$

where  $Sc$  is the Schmidt number of the given gas in freshwater at *in-situ* water temperature computed according the algorithms given by Waninkhof (1992).  $k_{600}$  was computed from wind speed using the parameterisation of Cole and Caraco (1998):

$$k_{600} = 2.07 + 0.215u^{1.7}$$

where  $u$  is the wind speed ( $\text{m s}^{-1}$ ).

The average daily  $u$  value on the day of sampling of each sampled pond was used. The  $u$  data were measured at the meteorological station of the Royal Meteorological Institute of St-Lambert (50.8408 °N, 4.4234 °E) in Brussels (located between 1 and 10 km from the sampled ponds) (retrieved from wow.meteo.be). The area-weighted average of  $F_G$  from the 22 sampled ponds (totaling a surface area of 34 ha) for each of the 4 seasons was averaged to obtain an annual value that was extrapolated to the total surface area (101 ha) of the all of the 158 urban ponds of the city of Brussels.

The emissions of  $\text{CH}_4$  and  $\text{N}_2\text{O}$  were expressed in  $\text{CO}_2$  equivalents ( $\text{CO}_2\text{-eq}$ ) by multiplying the respective fluxes by global warming potential (GWP) values of 34 for  $\text{CH}_4$  and 298 for  $\text{N}_2\text{O}$  corresponding to a time horizon of 100 years (Myrhe et al., 2013).

## 2.6. Statistical analysis

The statistical analyses were conducted using R version 4.1.1 (2022) (R Core Team, 2022) and graphs were produced with GraphPad Prism v9. Prior to analysis, data underwent logarithmic or square root transformations to ensure normality. Shapiro tests were performed to assess the normality of the distribution.

To investigate relationships between variables, quantile regressions were performed with the *quantreg* package v5.95 (Koenker, 2005). Quantile regressions were chosen over linear regressions due to their ability to provide a more comprehensive understanding of potential causal relationships in ecological processes (Cade and Noon, 2003). Significance levels for the quantile regression were determined using Wald statistical tests.

For comparisons of medians in the boxplots, permutational multivariate analysis of variance (PERMANOVA) on each Bray-Curtis distance matrix with 999 permutations was performed. A post-hoc test was performed to establish significant differences between sample pairs. For multiple comparisons,  $p$ -values were adjusted using the Bonferroni correction. Simultaneously, a test for homogeneity of multivariate dispersions (PERMDISP) was conducted. This test allowed for the examination of dispersion effects independent of location effects, as significant differences could be attributed to variations in within-group dispersion rather than differences in medians values among the groups (Anderson, 2006). PERMANOVA and PERDISP were performed using the *vegan* package v2.6.4 (Oksanen et al., 2013).

## Data availability

The time-sampled and georeferenced data-set presented in this paper is publicly available (Bauduin et al., 2024).

## 3. Results

### 3.1. Seasonal variations of meteorological conditions and GHGs

In 2022, the average air temperature in Brussels was 12.2 °C, above

the average of 11.0 °C for the 1991–2020 period. With the exception of April, September and December, air temperature monthly averages were above the reference value for the 1991–2020 period. A total of 701 mm of rain fell in Brussels (837 mm for the 1991–2020 period), during 149 days (190 days for the 1991–2020 period). The year 2022 was the fourth driest and the first (ex-aequo with 2020) warmest year of the current reference period. During the sampling period from 22/11/21 to 18/08/22, the air temperature and wind speed averaged 11.9 ± 6.3 °C and 0.6 ± 0.6  $\text{m s}^{-1}$ , respectively, and the total precipitation was 321 mm in the city of Brussels (Fig. 2A). Air temperature was highest in summer (22.2 ± 1.6 °C) and lowest in fall (6.1 ± 0.7 °C). The highest wind speed was in spring (Fig. 2B) (1.7 ± 0.5  $\text{m s}^{-1}$ ). In the 15 days prior to sampling, it rained a total of 13 mm in fall, 53 mm in winter, 13 mm in spring, and less than 1 mm in summer.

During the four sampling periods,  $\text{pCO}_2$  averaged 3667 ± 2904 ppm,  $\text{CH}_4$  concentration averaged 2833 ± 4178  $\text{nmol L}^{-1}$ , and % $\text{N}_2\text{O}$  averaged 273 ± 662‰ in the 22 sampled ponds in the city of Brussels. The maximum  $\text{pCO}_2$  value was observed in fall (15,029 ppm) and the minimum value in summer (121 ppm). Median  $\text{pCO}_2$  was higher in fall than during the other seasons and was lower in winter than spring (Fig. 3A). The maximum and minimum  $\text{CH}_4$  concentration values were both observed in summer, 29,190 and 10  $\text{nmol L}^{-1}$ , respectively (Fig. 3B). The  $\text{CH}_4$  concentrations showed seasonal variations, with significantly lower median concentration in winter than other seasons, and higher concentrations during spring and summer (Fig. 3B). The minimum and maximum values of % $\text{N}_2\text{O}$  were both observed during summer (0 and 10,354 ‰) (Fig. 3C). The median concentration of % $\text{N}_2\text{O}$  was lower during summer than fall and winter. The % $\text{N}_2\text{O}$  values showed a higher dispersion during summer than other seasons (Fig. 3C). Undersaturation of  $\text{CO}_2$  with respect to atmospheric equilibrium was observed only on 7 occurrences (out of 88 observations), during spring (2 times) and summer (5 times). For  $\text{N}_2\text{O}$ , undersaturation with respect to atmospheric equilibrium was observed at each season, 3 times in fall, 5 times in winter, 7 times in spring and 10 times during summer.  $\text{CH}_4$  concentrations were always above saturation.

The average, median, minimum and maximum values of ancillary variables (% $\text{O}_2$ , Chl- $\alpha$ , SRP,  $\text{Ptot}$ ,  $\text{NH}_4^+$ ,  $\text{NO}_3^-$  and  $\text{NO}_2^-$ ) are given in Table S2. The median % $\text{O}_2$  values were significantly lower in fall than in the other seasons (Table S2). The median Chl- $\alpha$  concentration value was significantly lower in winter than in fall and the highest concentrations were measured in summer, when values were the most variable. There were no differences between seasons for SRP.  $\text{Ptot}$  had higher concentrations in spring and summer than in fall and winter. DIN concentrations were significantly higher in fall and winter than during spring and summer.  $\text{NH}_4^+$ ,  $\text{NO}_3^-$  and  $\text{NO}_2^-$  concentrations were significantly higher in fall than during the other seasons.  $\text{pCO}_2$ ,  $\text{CH}_4$  concentration and % $\text{N}_2\text{O}$  were negatively related to % $\text{O}_2$  (Fig. 4A, 4G, 4M).  $\text{CH}_4$  concentration was positively related to water temperature (Fig. 4H) and % $\text{N}_2\text{O}$  was negatively related to water temperature (Fig. 4N). There was no relation between  $\text{pCO}_2$  and water temperature (Fig. 4B), nor Chl- $\alpha$  concentration (Fig. 4C).  $\text{pCO}_2$  was positively related to SRP (Fig. 4E).  $\text{CH}_4$  was negatively related to Chl- $\alpha$  (Fig. 4I). There was a positive correlation between  $\text{CH}_4$  and  $\text{Ptot}$  (Fig. 4L), that was also observed during each individual season, except in winter (Fig. S2A–S2D). The negative relation observed between  $\text{CH}_4$  and DIN (Fig. 4J) could be spurious and be attributed to parallel seasonal changes of both variables, as there were no correlations between  $\text{CH}_4$  and DIN when analysed independently for each season, except in spring (Fig. S2E–S2H). % $\text{N}_2\text{O}$  was positively correlated to DIN for the whole dataset (Fig. 4P) as well as for each season analysed independently (Fig. S2I–S2L). % $\text{N}_2\text{O}$  was statistically more strongly correlated to  $\text{NO}_2^-$  (Fig. 5C) and  $\text{NO}_3^-$  (Fig. 5D) than to  $\text{NH}_4^+$  (Fig. 5B). % $\text{N}_2\text{O}$  was negatively related to  $\text{O}_2$ :DIN (Fig. 5E),  $\text{O}_2$ : $\text{NO}_2^-$  (Fig. 5G) and  $\text{O}_2$ : $\text{NO}_3^-$  (Fig. 5H) but unrelated to  $\text{O}_2$ : $\text{NH}_4^+$  (Fig. 5F).

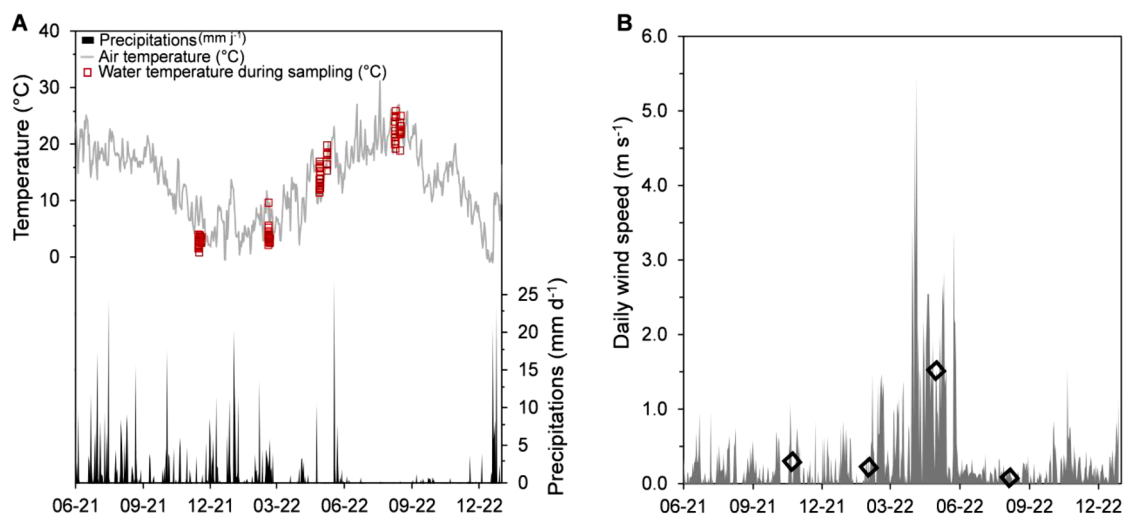


**Fig. 2.** Daily mean air temperature (light grey line), daily precipitation (black line) (A) and daily wind speed (dark grey, right) (B). The empty red squares on (A) indicate the *in-situ* water temperature during sampling and the empty black diamonds on (B) indicate the average wind during each sampling period. Meteorological data were obtained from crowdsourcing platform of the Royal Belgian Meteorological Institute (wow.meteo.be) at the Brussels–Woluwe Saint Lambert station (50.8408 °N, 4.4234 °E).

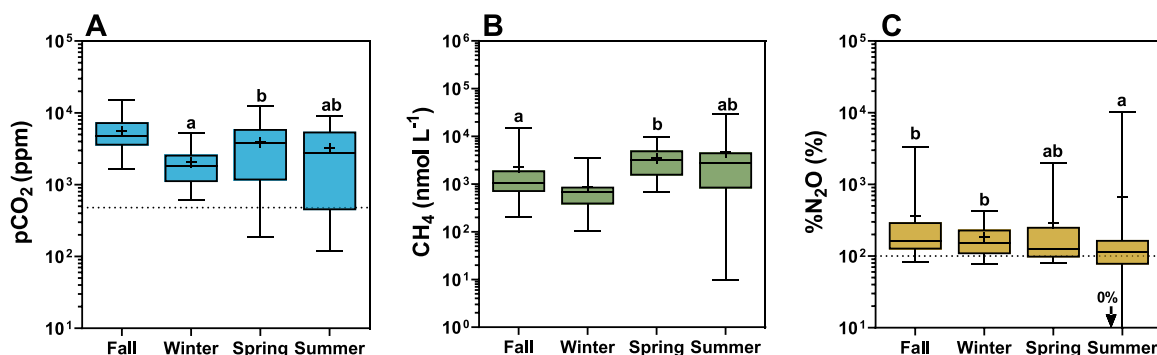


**Fig. 3.** Seasonal variations of partial pressure of CO<sub>2</sub> (pCO<sub>2</sub> in ppm) (A); dissolved CH<sub>4</sub> concentration (CH<sub>4</sub> in nmol L<sup>-1</sup>) (B) and N<sub>2</sub>O saturation level (%N<sub>2</sub>O in%) (C) in 22 ponds in the city of Brussels during 4 seasons. Dashed lines indicate the equilibrium with atmosphere (493 ppm for pCO<sub>2</sub> (mean of measurements) and 100 % for %N<sub>2</sub>O). Box plots show median (horizontal line), mean (cross), and 25–75 % percentiles (box limits). Whiskers extend from min to max. The common letters above the box plots indicate groups that are not significantly different (Permanova). Statistical results of Permanova and Betadisper are summarized in Table S5.

### 3.2. Spatial variations of GHGs

As pond perimeter ( $r = 0.90$ ,  $p < 0.0001$ ) and depth ( $r = 0.45$ ,  $p = 0.014$ ) were correlated to surface area; hereafter, only relationships between GHGs and pond surface area are presented (Fig. 6A, 6E, 6I). Both pCO<sub>2</sub> and %N<sub>2</sub>O were negatively related to pond surface area (Fig. 6A, 6I) and CH<sub>4</sub> was positively related to pond surface area (Fig. 6E). The ponds closer to the city center had lower CH<sub>4</sub> concentrations (Fig. 6F) and higher %N<sub>2</sub>O (Fig. 6J) than the ponds closer to the periphery of the city. %N<sub>2</sub>O values showed a higher dispersion in small ponds than larger ponds and in ponds closer to the city center compared to the periphery of the city. pCO<sub>2</sub> did not show a clear pattern with regards to the city center (Fig. 6B). DIN, NO<sub>3</sub><sup>-</sup> and NO<sub>2</sub><sup>-</sup> concentrations decreased with distance from the city center but not NH<sub>4</sub><sup>+</sup> (Fig. 7). Atmospheric nitrogen dioxide (NO<sub>2</sub>) concentration decreased with distance from the city center (Fig. 7E). %N<sub>2</sub>O was positively correlated to the atmospheric NO<sub>2</sub> concentration (Fig. 7F). Elevated CH<sub>4</sub> concentrations were observed in ponds with higher macrophyte cover (Fig. 6G). Ponds with high macrophyte cover were located farther away from the city center (Fig. S3A), had larger surface areas (Fig. S3B), and lower residence times (Fig. S3C). Ponds with high macrophyte cover exhibited lower concentrations of DIN and Chl-*a* than ponds with low macrophyte cover (Fig. S3D,E). Ponds with high and low macrophyte cover had no

difference in SRP and P<sub>tot</sub> concentration (Figs. S3F,G). No significant correlation was observed between Chl-*a* and distance from city center (Fig. S4).

### 3.3. Fluxes of GHGs

The mean and median concentrations of the three GHGs in the sampled ponds were consistently higher than their respective equilibrium concentrations (Fig. 3). Consequently, the sampled ponds were sources of GHGs to the atmosphere during all four seasons, although negative flux values were observed on some rare occasions (Fig. S5). Seasonal variations of the GHG fluxes mirrored those of the respective concentrations because of modest variations of wind speed and computed  $k_{600}$ , although higher fluxes were observed during spring characterized by the highest daily wind speeds (Fig. S5A).

In terms of GHG emissions expressed in CO<sub>2</sub> equivalents, CO<sub>2</sub> was the dominant GHG emitted, with a median annual emission to the atmosphere of 732 g CO<sub>2</sub> m<sup>-2</sup> yr<sup>-1</sup>. Median annual emission of CH<sub>4</sub> and N<sub>2</sub>O was 97 and 9 g CO<sub>2</sub>-eq m<sup>-2</sup> yr<sup>-1</sup>, respectively. CO<sub>2</sub> contributed to 88 % of the total CO<sub>2</sub> equivalent emissions, CH<sub>4</sub> contributed to 11 %, and N<sub>2</sub>O contributed to 1 %. The total annual diffusive emissions of CO<sub>2</sub>, CH<sub>4</sub>, and N<sub>2</sub>O amounted to 0.8 kT of CO<sub>2</sub>-eq for all of the ponds in the city of Brussels ( $n = 158$ ) (Fig. 8).

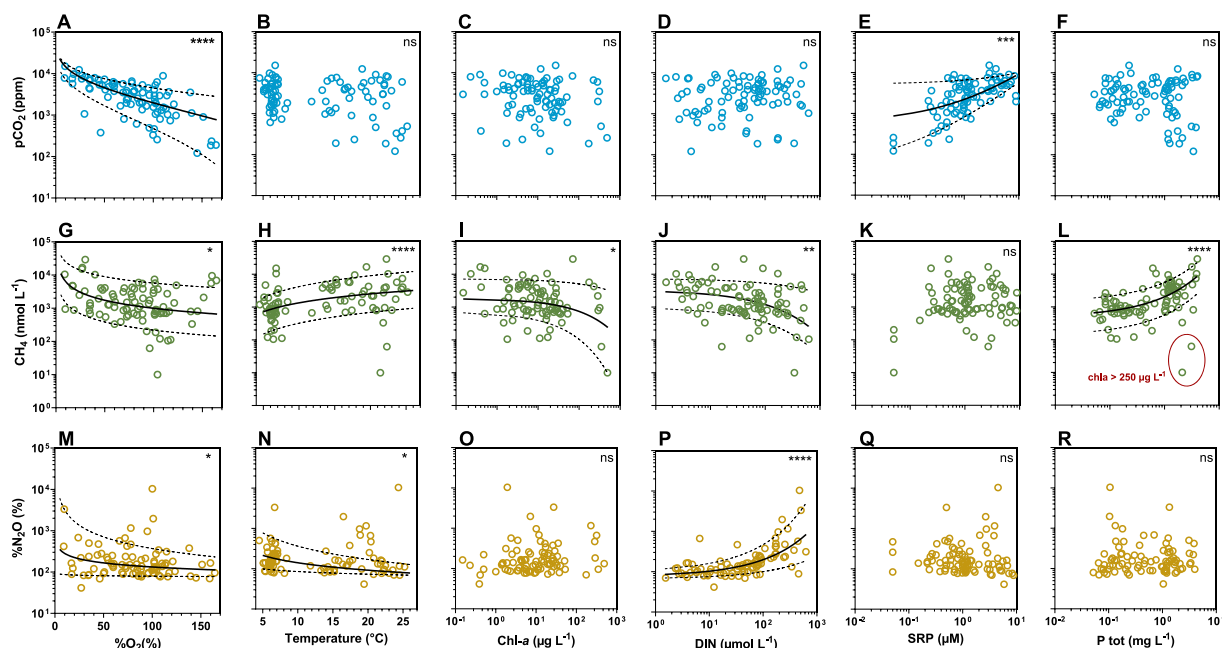


**Fig. 4.** Partial pressure of CO<sub>2</sub> (pCO<sub>2</sub>, ppm), dissolved CH<sub>4</sub> concentration (CH<sub>4</sub>, nmol L<sup>-1</sup>), and N<sub>2</sub>O saturation level (%N<sub>2</sub>O,%) versus oxygen saturation level (%O<sub>2</sub>, %), water temperature (°C), concentration of chlorophyll-a (Chl-a, in µg L<sup>-1</sup>), concentration of dissolved inorganic nitrogen (DIN= NH<sub>4</sub><sup>+</sup> + NO<sub>2</sub><sup>-</sup> + NO<sub>3</sub><sup>-</sup>, in µmol L<sup>-1</sup>), concentration of soluble reactive phosphorus (SRP, in µmol L<sup>-1</sup>) and total phosphorus concentration (P tot, mg L<sup>-1</sup>) in 22 ponds in the city of Brussels during 4 seasons. Median quantile regression shown as solid lines, 25th-75th quantile regression as dashed lines. Significance indicated by ns (non-significant) \* (p<0.05), \*\* (p<0.01), \*\*\* (p<0.0001). Statistical results of quantile regressions are summarized in Table S7.

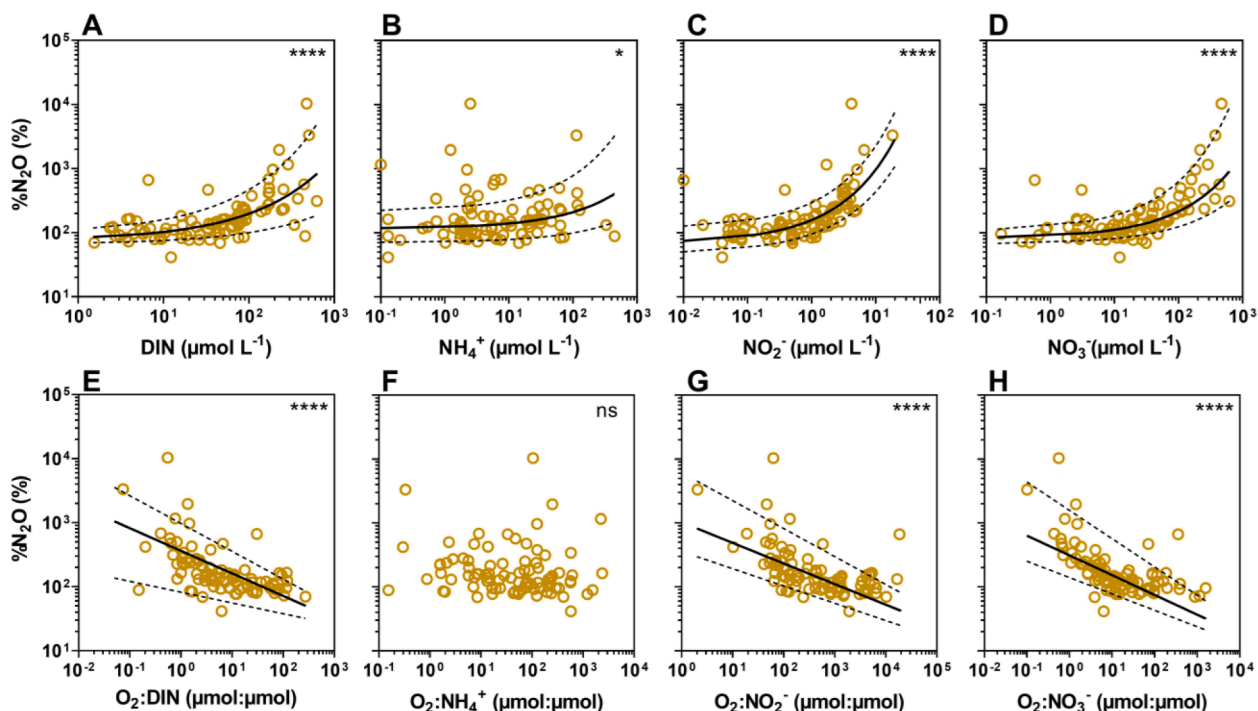


**Fig. 5.** N<sub>2</sub>O saturation level (%N<sub>2</sub>O,%) versus dissolved inorganic nitrogen (DIN= NH<sub>4</sub><sup>+</sup> + NO<sub>2</sub><sup>-</sup> + NO<sub>3</sub><sup>-</sup>, in µmol L<sup>-1</sup>) (A), ammonium concentration (NH<sub>4</sub><sup>+</sup>, µmol L<sup>-1</sup>) (B), nitrite concentration (NO<sub>2</sub><sup>-</sup>, µmol L<sup>-1</sup>) (C), nitrate concentration (NO<sub>3</sub><sup>-</sup>, µmol L<sup>-1</sup>) (D), ratio of dissolved inorganic nitrogen (DIN= NH<sub>4</sub><sup>+</sup> + NO<sub>2</sub><sup>-</sup> + NO<sub>3</sub><sup>-</sup>, in µmol L<sup>-1</sup>) to dissolved oxygen (O<sub>2</sub>, in µmol L<sup>-1</sup>) (E), ratio of NH<sub>4</sub><sup>+</sup> to O<sub>2</sub> (µmol:µmol) (F), ratio of NO<sub>2</sub><sup>-</sup> to O<sub>2</sub> (µmol:µmol) (G), ratio of NO<sub>3</sub><sup>-</sup> to O<sub>2</sub> (µmol:µmol) (H) in 22 sampled ponds in the city of Brussels during 4 seasons. Median quantile regression shown as solid lines, 25th-75th quantile regression as dashed lines. Significance indicated by \* (p<0.05), \*\*\*\* (p<0.0001). Statistical results of quantile regressions are summarized in Table S6.

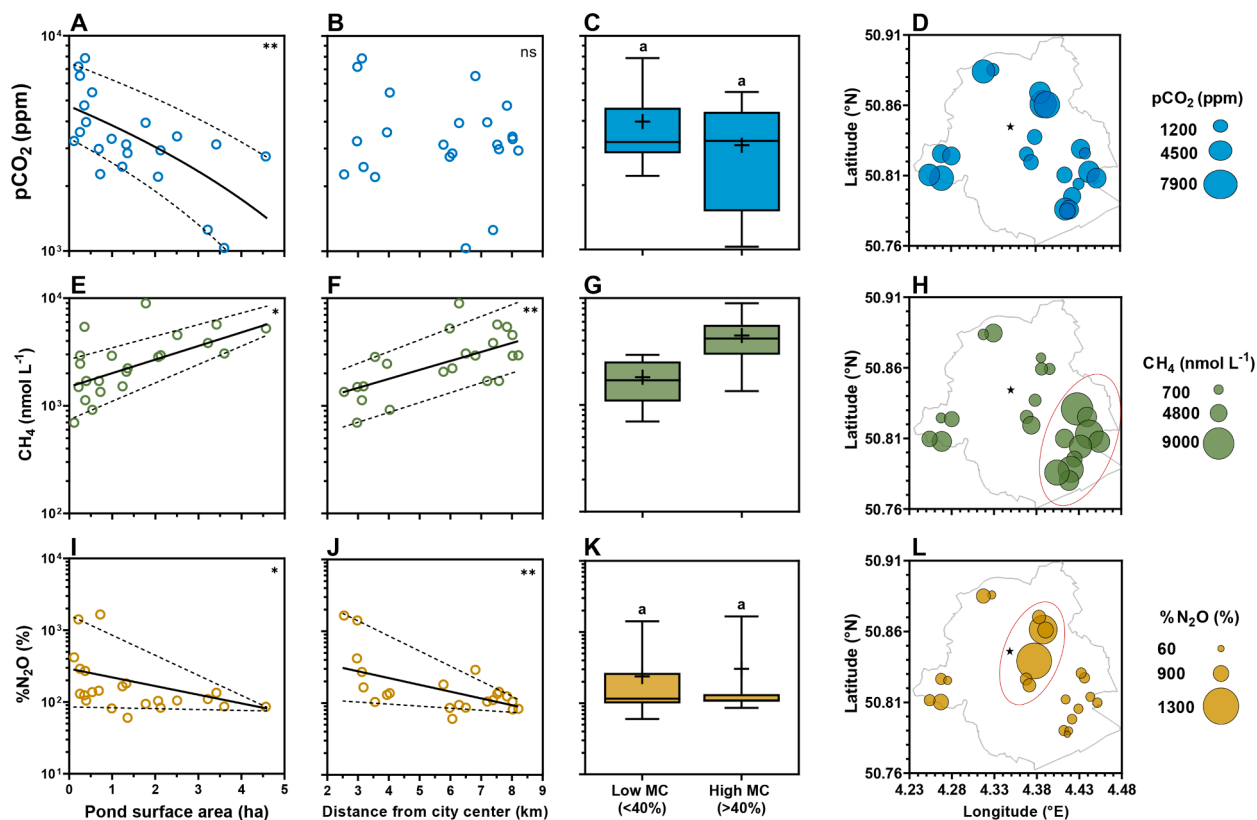


**Fig. 6.** Median quantile regressions of mean partial pressure of CO<sub>2</sub> (pCO<sub>2</sub>, ppm), dissolved CH<sub>4</sub> concentration (CH<sub>4</sub>, nmol L<sup>-1</sup>) and N<sub>2</sub>O saturation level (%N<sub>2</sub>O, %) as function of surface area (A, E, I) and distance from city center (B, F, J) and boxplots of mean GHG with low (<40%, n = 14) and high (>40%, n = 8) macrophyte cover (MC) (C, G, K). Median quantile regression shown as solid lines, 25th-75th quantile regression as dashed lines. Significance indicated by ns (non-significant) \* (p < 0.05), \*\* (p < 0.01). Box plots show median (horizontal line), mean (cross), and 25–75 % percentiles (box limits). Whiskers extend from min to max. The common letters above the box plots indicate groups that are not significantly different (Permanova). Graphs D, H, L represent respectively mean pCO<sub>2</sub> (ppm), CH<sub>4</sub>, (nmol L<sup>-1</sup>) and %N<sub>2</sub>O (%) for each pond during the four spatial surveys plotted against coordinates (°E, °N). City perimeter shown in light grey, city center (50.8504°N, 4.3487°E) marked with star. Red circles evidence zones with highest values of CH<sub>4</sub> concentrations and %N<sub>2</sub>O. Statistical results of quantile regressions are summarized in Table S6. Statistical results of Permanova and Betadisper are summarized in Table S7.

## 4. Discussion

### 4.1. Seasonal variations

Seasonal variations of dissolved CO<sub>2</sub> in lacustrine systems at mid and high latitudes depend on the seasonal alternation between periods of net ecosystem heterotrophy and periods when the aquatic ecosystem evolves to more autotrophic conditions. This seasonal alternation depends on light conditions, with a higher aquatic primary production in spring and summer. Light conditions co-vary with temperature, and warmer conditions coincide seasonally with the sunnier conditions in summer. Allochthonous organic matter inputs from the watershed can also vary seasonally and are usually stronger in fall and winter than spring and summer.

In the sampled ponds of the city of Brussels, the overall negative relation between pCO<sub>2</sub> and %O<sub>2</sub> (Fig. 4A) reflected an alternation between autotrophy-heterotrophy (balance between photosynthesis and community respiration), as also observed in other studies in rivers and lakes (Borges et al., 2015, 2018). This confirmed by the observed relationship between pCO<sub>2</sub> and SRP (Fig. 4F) that may reflect the uptake of nutrients by autotrophic groups leading to the lowering of SRP and pCO<sub>2</sub>, and, conversely, high SRP and pCO<sub>2</sub> resulting from the degradation of OM in the water column and sediments (Alleson et al., 2020). The pCO<sub>2</sub> values in the sampled ponds of the city of Brussels were highest in fall and lowest in summer. In fall, the senescence of photosynthetic organisms, induced by a decrease in light intensity and water temperatures, will lead to a large amount of potentially degradable

autochthonous OM (Bartosiewicz et al., 2021), which will be respired and lead to higher pCO<sub>2</sub> in fall than in winter and summer. The input in fall of allochthonous OM to ponds is increased with leaf fall from surrounding trees (Sønderup et al., 2016) and with runoff due to higher precipitation. In spring, the occurrence of aquatic primary production in response to the increase of the photoperiod and water temperature, lead to a CO<sub>2</sub> consumption and O<sub>2</sub> production.

In summer, the median (average) pCO<sub>2</sub> was not significantly different compared to other seasons, but there was a higher dispersion of the values that explained the lack of relation between pCO<sub>2</sub> and water temperature and Chl-*a* (Fig. 4B, 4C), unlike CH<sub>4</sub> and %N<sub>2</sub>O that correlated to water temperature (Fig. 4H, 4N). The high dispersion of pCO<sub>2</sub> values in summer may be attributed to sampling different stages of phytoplankton development in various ponds during the summer campaign (Fig. S4). Low pCO<sub>2</sub> values were observed in ponds where phytoplankton was blooming and high pCO<sub>2</sub> values were observed in ponds where phytoplankton was senescent. The relation of pCO<sub>2</sub> and Chl-*a* was further complicated by the variable density of macrophyte cover among the different sampled ponds. High macrophyte cover corresponded to low Chl-*a* concentrations, while low macrophyte cover corresponded to higher Chl-*a* levels (Fig. S3D).

Low %O<sub>2</sub> values in the water column indicate a generalized net heterotrophy within the sampled ponds including the sediments and therefore also a high methanogenesis, leading to an overall negative relation between CH<sub>4</sub> and %O<sub>2</sub> (Fig. 4G), as also observed in other urban ponds (Audet et al., 2020; Peacock et al., 2021). Since methanogenesis occurs in sediments rich in organic matter, seasonal variations of

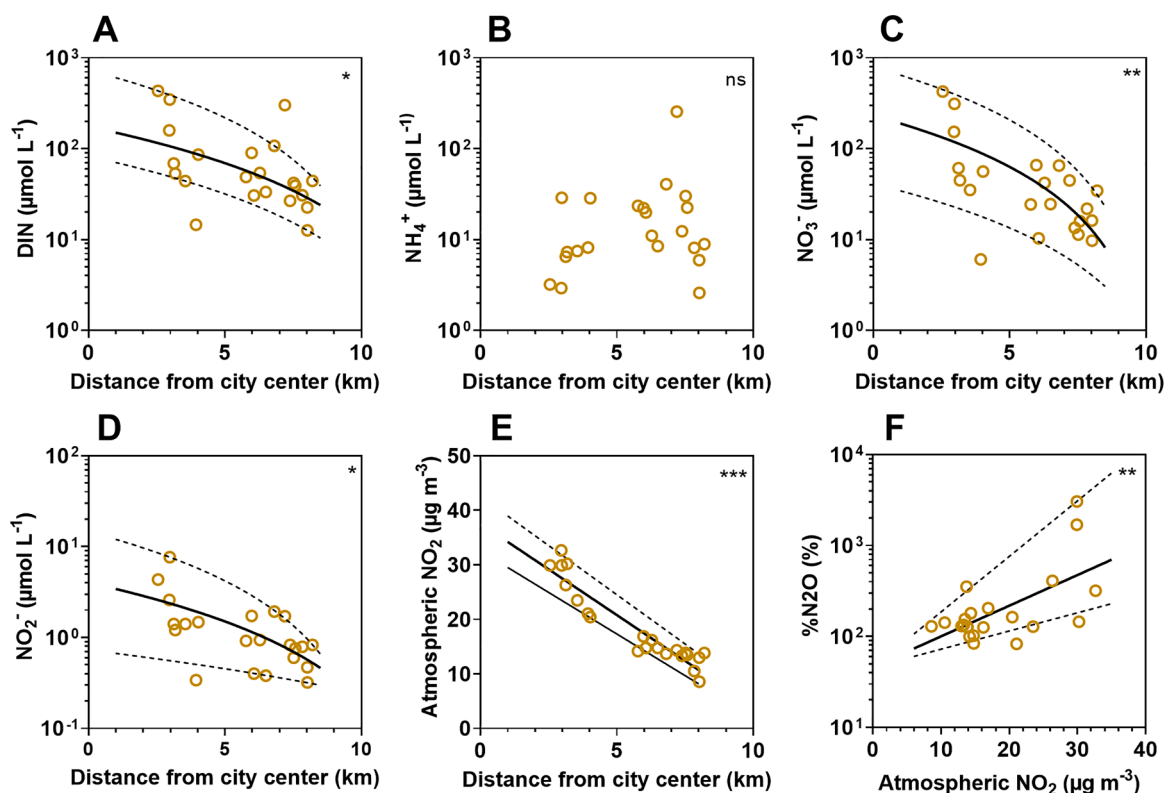


**Fig. 7.** Mean dissolved inorganic nitrogen (DIN=  $\text{NH}_4^+ + \text{NO}_2^- + \text{NO}_3^-$ , in  $\mu\text{mol L}^{-1}$ ) (A), ammonium ( $\text{NH}_4^+$ , in  $\mu\text{mol L}^{-1}$ ) (B), nitrite ( $\text{NO}_2^-$ , in  $\mu\text{mol L}^{-1}$ ) (C), nitrate ( $\text{NO}_3^-$ , in  $\mu\text{mol L}^{-1}$ ) (D), and atmospheric  $\text{NO}_2$  ( $\mu\text{g m}^{-3}$ ) (E) concentrations as function of the distance from city center (50.8504°N, 4.3487°E) in 22 ponds in the city of Brussels during 4 seasons.  $\text{N}_2\text{O}$  saturation level (% $\text{N}_2\text{O}$ ,%) as function of atmospheric  $\text{NO}_2$  concentration ( $\mu\text{g m}^{-3}$ ) (F). Median quantile regression shown as solid lines, 25th-75th quantile regression as dashed lines. Significance (ns non-significant, \*  $p < 0.05$ , \*\*  $p < 0.01$ ) indicated top right. Statistical results of quantile regressions are summarized in Table S6. The atmospheric nitrogen dioxide ( $\text{NO}_2$ ) concentration ( $\mu\text{g m}^{-3}$ ) was extracted from the Curieuzenair initiative, which analyzed 2483 air samples in September 2021 covering the whole of the city of Brussels with a homogeneous distribution (<https://curieuzenair.brussels/en/the-results/>). Each data point corresponds to the average value of the six atmospheric  $\text{NO}_2$  stations closest to each sampled pond, a distance between 50 and 450 m.

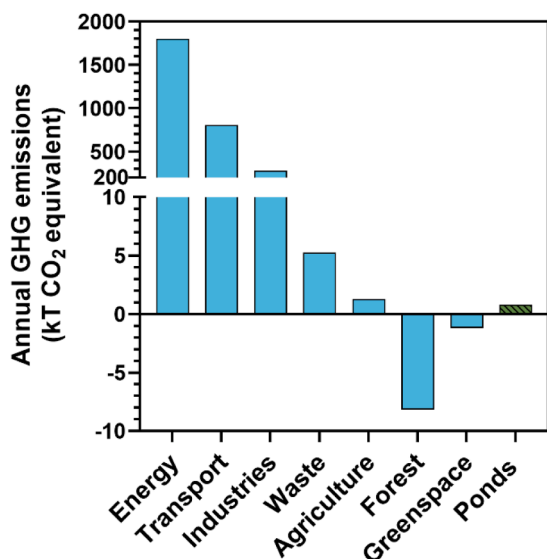


**Fig. 8.** Official inventory of annual emissions of greenhouse gases (kT CO<sub>2</sub> equivalents per year) for the city of Brussels in 2020 (<https://environnement.brussels>) Energy (residential/tertiary buildings), Transport (road), Industry (industrial processes and product use), Waste (mainly wastewater treatment), Agriculture (few soils), Forest (mainly Sonian forest), greenspace (private and public gardens, grassland) and diffusive emissions estimated from Brussels ponds (Ponds) in this study (2021–2022). The specific budget for each GHG is given in Table S4.

methanogenesis are very strongly dependent on temperature variations (Zeikus and Winfrey, 1976; Yvon-Durocher et al., 2014; Chen et al., 2021). Consequently, there was also a highly significant positive correlation between CH<sub>4</sub> and water temperature (Fig. 4H). There is a highly significant positive correlation between P<sub>tot</sub> and CH<sub>4</sub>, as in other urban ponds (Peacock et al., 2019; Rabaey and Cotner, 2022), probably reflecting the delivery of fresh, labile organic matter to sediments enhancing methanogenesis (Grasset et al., 2021; Gruca-Rokosz and Cieřla, 2021; Nijman et al., 2022). P<sub>tot</sub> was similar in ponds with high and low macrophyte cover (Fig. S3G), indicating P<sub>tot</sub> gives a measure of potentially degradable OM from both phytoplankton and macrophytes. Consequently, P<sub>tot</sub> was higher in spring and summer (Table S2), when primary production from phytoplankton and macrophytes is highest.

$\text{N}_2\text{O}$  in lakes and ponds results from nitrification and denitrification that show seasonal variations, mainly as a function of DIN availability and O<sub>2</sub> conditions (in particular in thermally stratified systems), as well as water temperature (Myrstener et al., 2016; Palacin-Lizarbe et al., 2018; Mander et al., 2021). Additionally, the yield of  $\text{N}_2\text{O}$  production from both nitrification and denitrification also depends on O<sub>2</sub> levels and water temperature. In the sampled ponds, % $\text{N}_2\text{O}$  was higher in fall than summer, as observed by Mander et al. (2021) in artificial wetlands. During fall, high heterotrophic degradation of organic matter and ammonification, combined with lower uptake of  $\text{NH}_4^+$  by phytoplankton, resulted in high concentrations of  $\text{NH}_4^+$  (Table S2). This led to high  $\text{N}_2\text{O}$  production from nitrification due to higher  $\text{NH}_4^+$  availability, and the  $\text{N}_2\text{O}$  yield from nitrification was possibly enhanced by low O<sub>2</sub> conditions (Rosamond et al., 2012; Soued et al., 2016). In spring and summer, the  $\text{NH}_4^+$  was assimilated by phytoplankton and there was substrate limitation for  $\text{N}_2\text{O}$  production by nitrification in the water column. The

combination of high and low nitrification in fall and spring, respectively explained the observed overall relationship between  $\%N_2O$  and  $NH_4^+$  (Fig. 5B).  $NO_2^-$  and  $NO_3^-$  are, respectively, intermediate and final product of the nitrification, which explained the observed overall relationship between  $\%N_2O$  and  $NO_2^-$  and  $NO_3^-$  (Figs. 5C, 5D) that was statistically more significant than the relation between  $\%N_2O$  and  $NH_4^+$ . Low  $O_2$  levels will favour  $N_2O$  production over  $NO_2^-$  production during nitrification (Goreau et al., 1980; Ni et al., 2011), leading to a negative relation between  $\%N_2O$  and  $O_2$ ; DIN,  $O_2$ ;  $NO_2^-$  and  $O_2$ ;  $NO_3^-$  (Fig. 5E, 5G, 5H). While the correlations between  $N_2O$  and  $NH_4^+$ ,  $NO_3^-$  and  $NO_2^-$  (Fig. 5B–5D) in the sampled ponds of the city of Brussels indicate the importance of nitrification in driving the variability of  $N_2O$ , denitrification should also have played a role in  $N_2O$  dynamics. An indication of this is given by the overall negative relationship between  $\%N_2O$  and water temperature (Fig. 4N), as the last step of denitrification is inhibited at low temperatures (Liao et al., 2018; Velthuis and Veraart, 2022), leading to an accumulation of  $N_2O$  in the water column during fall and winter. A pattern of higher  $N_2O$  levels during wintertime was also observed in boreal lakes and attributed to the effect of temperature on the  $N_2O$  yield from denitrification (Kortelainen et al., 2020).

#### 4.2. Spatial variations in GHGs

The levels of  $CO_2$  and  $CH_4$  in lakes vary as a function of lake size (Lapierre and del Giorgio, 2012; Kankaala et al., 2013; Raymond et al., 2013; Holgerson and Raymond, 2016; Casas-Ruiz et al., 2021; Borges et al., 2022; Chiriboga et al., 2024) as well as land cover (Maberly et al., 2013). Combined lake size and land cover determine relative levels of allochthonous organic matter inputs to aquatic systems and the general balance of autotrophy and heterotrophy largely determining  $CO_2$  levels (del Giorgio and Peters, 1994), as well as benthic methanogenesis. The size of the water body will also largely determine the relative importance of soil-water and ground-water inputs of  $CO_2$  and  $CH_4$  (Weyhenmeyer et al., 2015; Olid et al., 2022). The size of the water body will also determine to a larger extent its depth, with smaller systems being in general shallower (Wetzel, 2001). Depth will in turn determine the degree of coupling between sedimentary processes and surface waters, as well as the possibly development of macrophytes. Yet, given the low number of studies, it has not been investigated if these general patterns established from studies in natural lakes and ponds can be applied to urban ponds. In urban ponds the catchment cover is obviously very different from more natural systems, and there is a very strong atmospheric nitrogen deposition. Inter-lake variations of  $N_2O$  have been less investigated than  $CO_2$  and  $CH_4$ , although DIN levels and depth are expected to exert a strong influence on  $N_2O$  lacustrine levels (Lauerwald et al., 2019; Borges et al., 2022).

The surface area of the sampled ponds was overall low and the range of variation was small (0.1–4.6 ha), so that other properties than pond size might have driven inter-system differences. The analysis of spatial patterns of GHGs in the sampled ponds was complicated by the fact that the smaller systems were located towards the center of city, and the larger ones at the periphery in contact with either cropland to the West and the Sonian forest to the East. Furthermore, the larger systems were characterized by a more important macrophyte cover.

The  $pCO_2$  values in the sampled ponds did not show a significant relation to the distance from the city center or macrophyte cover (Fig. 6B, 6C). However, the  $pCO_2$  values were significantly higher in the smaller systems than the larger ones (Fig. 6A). This agrees with several studies at local, regional or global scales showing a negative relation between  $pCO_2$  and lake surface area (Lapierre and Del Giorgio, 2012; Kankaala et al., 2013; Raymond et al., 2013; Holgerson and Raymond, 2016; Casas-Ruiz et al., 2021). The causes of such relations are related to the overall influence of lake size on inputs from the landscape and lake carbon cycling and have been discussed in detail in several other studies (del Giorgio and Peters, 1994; Sand-Jensen and Staehr, 2007; Borges et al., 2022).

The  $CH_4$  concentration in the sampled ponds was significantly higher in the larger systems than the smaller ones (Fig. 6E). Several studies reported a negative correlation between  $CH_4$  concentration and lake size (surface and/or depth) across spatial scales (local to global) (Borges et al., 2011; Kankaala et al., 2013; Holgerson and Raymond, 2016; Borges et al., 2022; Chiriboga et al., 2024), yet one study reported no relationship (Peacock et al., 2019) and another a positive correlation (Rabaey et al., 2022). The positive relationship between  $CH_4$  concentration and pond size in the ponds of the city of Brussels was probably indirect and reflected another driver. The relationship of  $CH_4$  concentrations in relation to the distance from the city center and to macrophyte cover was statistically more significant than to surface area (Fig. 6E–6G). We hypothesize that macrophyte cover was the predominant driver (given the stronger statistical significance) that was itself a function of distance from the city center. The statistically weak negative relationship between Chl-*a* and  $CH_4$  (Fig. 4J) could reflect the fact that ponds with high macrophyte cover tended to exhibit lower Chl-*a* concentrations (Fig. S3D) but had significantly higher  $CH_4$  concentrations (Fig. 6G).

Submerged macrophytes have a complex impact on  $CH_4$  dynamic in lakes and ponds, as synthesized by Bastviken et al. (2023), with both positive and negative effects on the  $CH_4$  emissions. In the urban ponds of the city of Brussels, the  $CH_4$  concentration was significantly higher in ponds with a high macrophyte cover (Fig. 6G), located in the periphery of the city and closer to the Sonian Forest (Fig. 6F, 6H). In addition to the potential positive impact of macrophytes on  $CH_4$ , the Sonian forest likely transfers allochthonous carbon as plant litter promoting  $CH_4$  production compared to other ponds. Litter from trees can induce sediment anoxia (Mehring et al., 2014) enhancing  $CH_4$  production. Yet, this potential additional input of allochthonous organic carbon from the Sonian Forest did not seem to affect the  $pCO_2$  in ponds for which the effect of size seemed more important.

The  $\%N_2O$  levels were significantly higher but also more variable in the sampled urban ponds closer to the city center than at the periphery of the city (Fig. 6J, 6L).  $\%N_2O$  was strongly correlated to DIN,  $NO_2^-$  and  $NO_3^-$  concentrations (Fig. 5) that were higher close to the city center (Fig. 7). The higher DIN,  $NO_2^-$  and  $NO_3^-$  concentrations in the city center could have resulted from higher N deposition as indicated by the pattern of atmospheric  $NO_2$  (Fig. 7E). No correlation was found with macrophyte cover (Fig. 6K), although the presence of macrophytes strongly influences nitrogen cycling in sediments (Barko et al., 1991; Choudhury et al., 2018; Dan et al., 2021; Ni et al., 2022) and could in theory potentially have affected  $N_2O$  levels.

#### 4.3. Comparison with other urban and natural ponds

There are only a few equivalent studies of GHG emissions in urban ponds for comparison (Table S3). We restricted the comparison to dissolved GHG concentrations rather than fluxes across the air-water interface. Fluxes measured with floating chambers and computed fluxes from  $k$  can provide diverging results, so are not necessarily comparable (Duchemin et al., 1999; Guérin et al., 2007; Klaus and Vachon, 2020; Erkkilä et al., 2018; Perolo et al., 2021). This is possibly related to measurement biases using floating chambers (Belanger and Korzun, 1991; Lorke et al., 2015; Vingiani et al., 2021), although the computation of  $k$  can be made with different parameterizations derived from several methods (including floating chambers) and that provide different values particularly at high wind speeds. It is unclear which wind parametrization is the most appropriate (Klaus and Vachon, 2020), in particular with regards to effects of size and fetch limitation (Waninkhof, 1992) which might become very important in small water bodies such as ponds (Holgerson et al., 2017; Jansen et al., 2020). We computed the fluxes from dissolved concentrations of  $CO_2$ ,  $CH_4$  and  $N_2O$  and the gas transfer velocity computed from the parameterization as a function of wind speed of Cole and Caraco (1998). The parametrization of Cole and Caraco (1998) was built from a large compilation of

deliberate tracer based estimates of  $k_{600}$  in 11 lakes with a wide range of maximum depth (1–109 m) and surface area (0.2–487 km<sup>2</sup>). The parametrization of Cole and Caraco (1998) parameterization as function of wind speed intrinsically integrates other sources of turbulence (night-time convection due to cooling) and fetch limitation, because it is built on compilation of repeated tracer measurements in several lakes with a wide range of size and depth. Yet, the parameterization of Cole and Caraco (1998) is based on  $k_{600}$  data acquired in water bodies with a surface area larger (>4 ha) than the ponds we sampled (0.1–4.6 ha), which admittedly introduces uncertainty in the computation of  $k_{600}$ . The computed  $k_{600}$  from the sampled ponds with the parametrization of Cole and Caraco (1998) ranged from 2.1 to 2.6 cm h<sup>-1</sup> in summer and spring, respectively. The overall annual average  $k_{600}$  value of 2.3 cm h<sup>-1</sup> was within the range of  $k_{600}$  values (0.9–3.0 cm h<sup>-1</sup>) reported by Holgerson et al. (2017) in four ponds located in a dense forest, with surface area ~0.02 ha. These four ponds located in a dense forest were smaller than the ponds we sampled (0.1–4.6 ha) that were located in recreational urban parks, hence, less sheltered from wind than in a dense forest. The values of computed  $k_{600}$  from the sampled ponds with the parametrization of Cole and Caraco (1998) are also comparable to the values of  $k_{600}$  used by Holgerson and Raymond (2016), in a global analysis of CO<sub>2</sub> and CH<sub>4</sub> emissions from ponds, of 1.5 cm h<sup>-1</sup> for ponds with a surface area <0.1 ha and of 2.0 cm h<sup>-1</sup> for ponds with a surface are of 0.1–1.0 ha.

The average of CH<sub>4</sub> dissolved concentrations (annual or summer average) in the sampled ponds of Brussels was comparable to the values reported in other urban ponds in the cities of Silkeborg (Denmark, Audet et al., 2020), Uppsala (Sweden, Peacock et al., 2019; Ray et al., 2023), Linköping (Sweden, Natchimuthu et al., 2014), Minnesota (United States, Rabaey and Cotner, 2022; Ray et al., 2023) and in Salaspils (Latvia, Ray et al., 2023). The average dissolved CO<sub>2</sub> concentrations in the sampled ponds was also equivalent to the values in the ponds of Silkeborg (average of 4 seasons) (Audet et al., 2020) and possibly lower in summer than the ponds in Uppsala (Peacock et al., 2019).

The extreme variability of CH<sub>4</sub> and CO<sub>2</sub> concentrations seasonally and among ponds indicated by the large values of the standard deviations was observed in all systems (Brussels, Silkeborg, Uppsala, Minnesota and Salaspils) and probably obscured differences among different studies that could have emerged from differences in inputs of allochthonous carbon and nitrogen, despite the differences in the size of the cities, as Brussels (> 1 million inhabitants) is larger than Silkeborg (<50,000 inhabitants) and Uppsala (140,000 inhabitants). The N<sub>2</sub>O concentration in the sampled ponds of Brussels was higher than values in the ponds of Silkeborg (average of 4 seasons) (Audet et al., 2020), which might be a consequence of a larger anthropogenic input of nitrogen from atmospheric deposition due to the larger size of the city of Brussels compared to Silkeborg. This was consistent with a higher value of the annual average NH<sub>4</sub><sup>+</sup> concentration in the ponds of Brussels (27±63 μmol L<sup>-1</sup>) compared to the ponds of Silkeborg (9 ± 14 μmol L<sup>-1</sup>, Audet et al., 2020). A stronger eutrophication (nitrogen levels) sustaining a higher primary production, might also explain potentially lower CO<sub>2</sub> concentrations in Brussels in summer than in Silkeborg and Uppsala (Table S3).

Concentrations of CO<sub>2</sub> and CH<sub>4</sub> in the sampled ponds of Brussels were >3 times higher than those in natural (non-urban) ponds of similar size reported by Holgerson and Raymond (2016) (Fig. 9). This confirms the emerging idea that artificial inland water bodies (agricultural reservoirs, urban ponds, storm-water retention basins, ...) have higher emission rates per m<sup>2</sup> than natural systems (Martinez-Cruz et al., 2017; Grinham et al., 2018; Herrero Ortega et al., 2019; Gorsky et al., 2019; Ollivier et al., 2019; Peacock et al., 2019, 2021; Webb et al., 2019). This seems to result from more important anthropogenic allochthonous inputs of carbon and nitrogen in artificial systems but might also reflect other differences compared to natural systems such as in hydrology (Clifford and Heffernan, 2018).

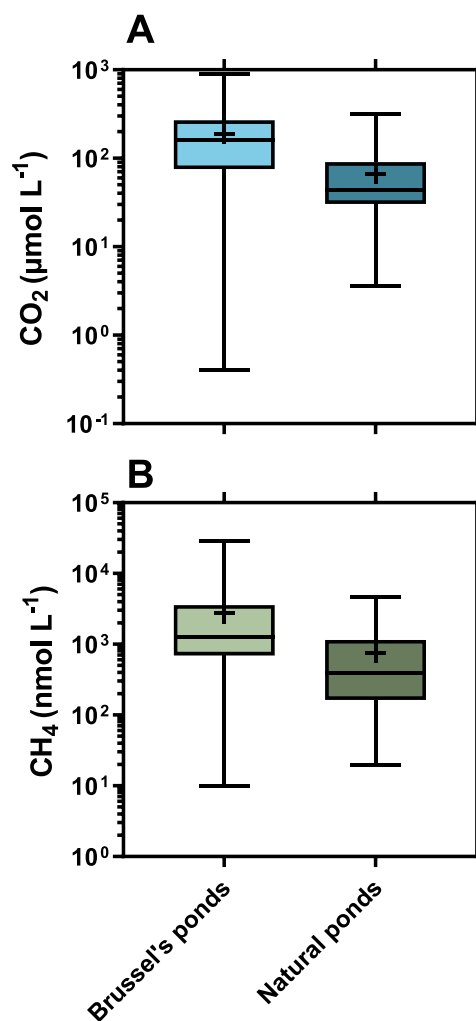


Fig. 9. dissolved CO<sub>2</sub> concentration (CO<sub>2</sub>, μmol L<sup>-1</sup>) (A) and dissolved CH<sub>4</sub> concentration (CH<sub>4</sub>, nmol L<sup>-1</sup>) (B) in 22 sampled ponds in Brussels during 4 seasons ( $n = 88$ ) and natural ponds of similar size reported by Holgerson and Raymond (2016) ( $n = 81$  for CO<sub>2</sub>,  $n = 53$  for CH<sub>4</sub>). Box plots show median (horizontal line), mean (cross), and 25–75 % percentiles (box limits). Whiskers extend from min to max. Both comparisons are significant based on Permanova test. Statistical results of Permanova and Betadisper are summarized in Table S5.

#### 4.4. Contribution of urban ponds to the GHG budget of the city of Brussels

The CO<sub>2</sub>, CH<sub>4</sub> and N<sub>2</sub>O air-water fluxes were converted into CO<sub>2</sub> equivalents and the average scaled to total surface area of ponds in the city of Brussels (101 ha). The diffusive emissions were dominated by CO<sub>2</sub> (88 %), followed by CH<sub>4</sub> (11 %) and N<sub>2</sub>O (1 %). The GHG emissions officially accounted from the city of Brussels are overwhelmingly dominated by CO<sub>2</sub> (99.1 %) with a very small contribution from N<sub>2</sub>O (0.6 %) and CH<sub>4</sub> (0.3 %). The relative additional contribution of emissions of GHG from ponds to the total urban emissions is different for each of the three GHGs individually (Table S4). The diffusive emissions from ponds correspond to a fraction of the other urban emissions of 1.2 % for CH<sub>4</sub>, 0.05 % for N<sub>2</sub>O and 0.03 % for CO<sub>2</sub>. The total annual GHG diffusive emissions from ponds of 0.8 kTCO<sub>2</sub>eq is several orders of magnitude lower and very marginal compared to the three major anthropogenic emissions in the city of Brussels such as energy (1804 kTCO<sub>2</sub>eq yr<sup>-1</sup>), transport (807 kTCO<sub>2</sub>eq yr<sup>-1</sup>), and industries (277 kTCO<sub>2</sub>eq yr<sup>-1</sup>) (Fig. 8). Ebullitive fluxes of CH<sub>4</sub> were measured in four ponds (Leybeek, Pêcheries Royales, Silex, Ten Reuken) during 2021,

2022, and 2023 and ranged from 0.0 to 59.2 mmol CH<sub>4</sub> m<sup>-2</sup> d<sup>-1</sup> (unpublished data). Based on an exponential relationship between ebullitive CH<sub>4</sub> and temperature in the 4 sampled ponds ( $n = 39$ ,  $r^2 = 0.54$ , not shown), we scaled the ebullitive CH<sub>4</sub> fluxes to all of ponds in the city of Brussels that summed correspond to an additional GHG emission of 0.2 kTCO<sub>2</sub>-eq yr<sup>-1</sup>. When additionally accounting for CH<sub>4</sub> ebullition, the total CH<sub>4</sub> emissions from the urban ponds (0.2 kTCO<sub>2</sub>-eq yr<sup>-1</sup>) correspond to 3.7 % of the total urban emissions of CH<sub>4</sub>. Yet, the total CH<sub>4</sub> emissions (including CH<sub>4</sub> ebullition) from the urban ponds only represented 0.01 % of the total GHG emissions of the city of Brussels (2885 kTCO<sub>2</sub>-eq yr<sup>-1</sup>). This was consistent with the contribution of CH<sub>4</sub> emissions from streams and ponds of 0.004 % to the total GHG emissions from the city of Berlin reported by Herrero Ortega et al. (2019). The total annual GHG emissions from urban ponds, (1.0 kTCO<sub>2</sub>-eq yr<sup>-1</sup> including CH<sub>4</sub> ebullition) is of the same order of magnitude as smaller GHG emissions such as waste (5.3 kTCO<sub>2</sub>-eq yr<sup>-1</sup>) and agriculture (1.3 kTCO<sub>2</sub>-eq yr<sup>-1</sup>). The total annual GHG emissions from urban ponds was nearly identical than the estimated sink of GHGs from urban green spaces (1.2 kTCO<sub>2</sub>-eq yr<sup>-1</sup>). Urban green spaces (parks and gardens) provide several ecosystem services reviewed by Pataki et al. (2011) including reducing or offsetting GHG emissions. Here, we showed that the emissions of GHGs from ponds almost fully balance the reported GHG sink reported for green spaces in the city of Brussels. As such, GHG emissions from ponds should be accounted among the negative consequences or tradeoffs of implementing green infrastructure, the so-called “ecosystem disservices” according to Pataki et al. (2011).

## 5. Conclusions

Our study showed that small urban ponds in the public parks of the city of Brussels emit CO<sub>2</sub>, CH<sub>4</sub> and N<sub>2</sub>O to the atmosphere. The GHG concentrations and emissions in the sampled ponds showed geographical variations that were partly related to differences in morphology (size) but also the position with regards to the city center, and the surrounding landscape for those in the urban periphery (cropland versus forest), as well as the presence of macrophytes. Smaller ponds received larger amounts of allochthonous carbon, either directly as CO<sub>2</sub> or as OM resulting in larger CO<sub>2</sub> production from respiration. Larger ponds emitted more CH<sub>4</sub> contrary to the pattern most commonly described in the literature. This effect was due to the presence of macrophytes and the proximity of the forest in larger ponds at the periphery of the city compared to the smaller ponds located closer to the city center. N<sub>2</sub>O levels were higher closer to the city center that we hypothesize resulting from a stronger atmospheric nitrogen deposition based on the patterns of atmospheric NO<sub>2</sub>.

Biological processes were the main drivers of GHG production, as showed from relationships of the three GHGs with water temperature, oxygen saturation and nutrients. CH<sub>4</sub> concentrations were positively related to temperature on seasonal time scales due to the dependence of methanogenesis on temperature, as usually observed in aquatic systems (Yvon-Durocher et al., 2014), including urban ponds (Bartosiewicz et al., 2016). On the contrary the N<sub>2</sub>O levels were negatively related to temperature possibly reflecting incomplete denitrification at low temperatures, although DIN levels also increased in winter, so it is difficult to separate the impact of both potential drivers.

The GHG emissions from the studied ponds were lower than the other GHG sources from the city such as road transport and building heating. However, urban green spaces are described as important carbon sinks by Pataki et al. (2011), but this sink was offset by emissions from the ponds within these same green spaces in the city of Brussels. CH<sub>4</sub> emissions from inland waters were incorporated in the latest IPCC assessment report (IPCC, 2019) and should now be included in current national inventories. We show that the total CH<sub>4</sub> emissions from the urban ponds (including diffusive and ebullitive components) correspond to a larger fraction of the total respective urban emissions (3.73 %) than CO<sub>2</sub> (0.05 %) and N<sub>2</sub>O (0.03 %). The emissions of GHGs from the urban

ponds were equivalent to the reported GHG sink reported for green spaces in the city of Brussels.

Audet et al. (2020) proposed to consider the GHG emissions from ponds in the overall GHG assessment of cities to provide a more comprehensive quantification of a city's carbon footprint and fully quantify the ecosystem services provided by urban green spaces. Yet, the total CO<sub>2</sub>, N<sub>2</sub>O, and CH<sub>4</sub> emissions (including CH<sub>4</sub> ebullition) from the urban ponds only represented 0.04 % of the total GHG emissions of the city of Brussels (2885 kTCO<sub>2</sub>-eq yr<sup>-1</sup>).

## Declaration of competing interest

The authors declare that they have no known competing financial interests or personal relationships that could have appeared to influence the work reported in this paper.

## Acknowledgements

TB received a funding from the Brussels-Capital Region's institute for the encouragement of scientific research and innovation (Innoviris) as part of the Smartwater project (ref. Innoviris RBC/2020-EPF-6 h) and also from the “Fonds pour la formation à la Recherche dans l'Industrie et dans l'Agriculture” (FRIA, Belgium). CH<sub>4</sub> and N<sub>2</sub>O analyses were done by Thomas Bousmanne and Ozan Efe. The analysis of total phosphorus was performed at the Institut Meurice, within the Department of Physical Chemistry and Catalysis at Labiris, under the supervision of Vincent Dubois and Grégory Ploeglaerts. AVB is a Research Director at the Fonds National de la Recherche Scientifique.

## References

- Allesson, L., Andersen, T., Dörsch, P., Eiler, A., Wei, J., Hessen, D.O., 2020. Phosphorus availability promotes bacterial DOC-mineralization, but not cumulative CO<sub>2</sub>-production. *Front. Microbiol.* 11, 569879 <https://doi.org/10.3389/fmicb.2020.569879>.
- Anderson, M.J., 2006. Distance-based tests for homogeneity of multivariate dispersions. *Biometrics* 62 (1), 245–253. <https://doi.org/10.1111/j.1541-0420.2005.00440.x>.
- Audet, J., Carstensen, M.V., Hoffmann, C.C., Lavaux, L., Thieme, K., Davidson, T.A., 2020. Greenhouse gas emissions from urban ponds in Denmark. *Inland Waters* 10 (3), 373–385. <https://doi.org/10.1080/20442041.2020.1730680>.
- Baliña, S., Sanchez, M.L., Izaguirre, I., del Giorgio, P.A., 2023. Shallow lakes under alternative states differ in the dominant greenhouse gas emission pathways. *Limnol. Oceanogr.* 68 (1), 1–13. <https://doi.org/10.1002/lno.12243>.
- Barko, J.W., Gunnison, D., Carpenter, S.R., 1991. Sediment interactions with submersed macrophyte growth and community dynamics. *Aquat. Bot.* 41 (1–3), 41–65. [https://doi.org/10.1016/0304-3770\(91\)90038-7](https://doi.org/10.1016/0304-3770(91)90038-7).
- Bartosiewicz, M., Laurion, I., Clayer, F., Maranger, R., 2016. Heat-wave effects on oxygen, nutrients, and phytoplankton can alter global warming potential of gases emitted from a small shallow lake. *Environ. Sci. Technol.* 50 (12), 6267–6275. <https://doi.org/10.1021/acs.est.5b06312>.
- Bartosiewicz, M., Maranger, R., Przytulska, A., Laurion, I., 2021. Effects of phytoplankton blooms on fluxes and emissions of greenhouse gases in a eutrophic lake. *Water Res.* 196, 116985 <https://doi.org/10.1016/j.watres.2021.116985>.
- Bastviken, D., Treat, C.C., Pangala, S.R., Gauci, V., Enrich-Prast, A., Karlson, M., Gålfalk, M., Romano, M.B., Sawakuchi, H.O., 2023. The importance of plants for methane emission at the ecosystem scale. *Aquat. Bot.* 184, 103596 <https://doi.org/10.1016/j.aquabot.2022.103596>.
- Bauduin, T., Gypens, N., Borges, A.V., 2024. Biogeochemical data from urban ponds in Brussels [Data set] Zenodo. <https://doi.org/10.5281/zenodo.10554478>.
- Belanger, T.V., Korzun, E.A., 1991. Critique of floating-dome technique for estimating reaeration rates. *J. Environ. Eng.* 117 (1), 144–150. [https://doi.org/10.1061/\(ASCE\)0733-9372\(1991\)117:1\(144\)](https://doi.org/10.1061/(ASCE)0733-9372(1991)117:1(144)).
- Betz, N.D., Groffman, P.M., 2013. Nitrogen deposition in and near an urban ecosystem. *Environ. Sci. Technol.* 47 (11), 6047–6051. <https://doi.org/10.1021/es400664b>.
- Bonetti, G., Limpert, K.E., Brodersen, K.E., Trevathan-Tackett, S.M., Carnell, P.E., Macreadie, P.I., 2022. The combined effect of short-term hydrological and N-fertilization manipulation of wetlands on CO<sub>2</sub>, CH<sub>4</sub>, and N<sub>2</sub>O emissions. *Environ. Pollut.* 294, 118637 <https://doi.org/10.1016/j.envpol.2021.118637>.
- Borges, A.V., Abril, G., Delille, B., Descy, J.P., Darchambeau, F., 2011. Diffusive methane emissions to the atmosphere from Lake Kivu (Eastern Africa). *J. Geophys. Res.* Biogeosci. 116 (G3) <https://doi.org/10.1029/2011JG001673>.
- Borges, A.V., Darchambeau, F., Lambert, T., Bouillon, S., Morana, C., Brouyère, S., Hakoun, V., Jurado, A., Tseng, H.C., Descy, J.P., Roland, F.A.E., 2018. Effects of agricultural land use on fluvial carbon dioxide, methane and nitrous oxide concentrations in a large European river, the Meuse (Belgium). *Sci. Total Environ.* 610, 342–355. <https://doi.org/10.1016/j.scitotenv.2017.08.047>.

- Borges, A.V., Darchambeau, F., Lambert, T., Morana, C., Allen, G.H., Tambwe, E., Bouillon, S., 2019. Variations in dissolved greenhouse gases (CO<sub>2</sub>, CH<sub>4</sub>, N<sub>2</sub>O) in the Congo River network overwhelmingly driven by fluvial-wetland connectivity. *Biogeosciences* 16 (19), 3801–3834. <https://doi.org/10.5194/bg-16-3801-2019>.
- Borges, A.V., Darchambeau, F., Teodoru, C.R., Marwick, T.R., Tamooh, F., Geeraert, N., Omengo, F.O., Guérin, F., Lambert, T., Morana, C., Okuku, E., Bouillon, S., 2015. Globally significant greenhouse-gas emissions from African inland waters. *Nat. Geosci.* 8 (8), 637–642. <https://doi.org/10.1038/ngeo2486>.
- Borges, A.V., Deirmendjian, L., Bouillon, S., Okello, W., Lambert, T., Roland, F.A.E., Razanamahandry, V.F., Voarintsoa, N.R.G., Darchambeau, F., Kimirei, I.A., Descy, J., Allen, G.H., Morana, C., 2022. Greenhouse gas emissions from African lakes are no longer a blind spot. *Sci. Adv.* 8 (25), eabi8716. <https://doi.org/10.1126/sciadv.abi8716>.
- Bowden, W.B., Glime, J.M., et Riis, T., 2017. *Macrophytes and Bryophytes. Methods in Stream Ecology: Third Edition.* Academic Press, pp. 1–494.
- Brans, K.I., Engelen, J.M., Souffreau, C., De Meester, L., 2018. Urban hot-tubs: local urbanization has profound effects on average and extreme temperatures in ponds. *Landsc. Urban Plan.* 176, 22–29. <https://doi.org/10.1016/j.landurbplan.2018.03.013>.
- Cade, B.S., Noon, B.R., 2003. A gentle introduction to quantile regression for ecologists. *Front. Ecol. Environ.* 1 (8), 412–420. [https://doi.org/10.1890/1540-9295\(2003\)001\[0412:AGITQR\]2.0.CO;2](https://doi.org/10.1890/1540-9295(2003)001[0412:AGITQR]2.0.CO;2).
- Casas-Ruiz, J.P., Jakobsson, J., del Giorgio, P.A., 2021. The role of lake morphometry in modulating surface water carbon concentrations in boreal lakes. *Environ. Res. Lett.* 16 (7), 074037 <https://doi.org/10.1088/1748-9326/ac0bc3>.
- Chen, H., Xu, X., Fang, C., Li, B., Nie, M., 2021. Differences in the temperature dependence of wetland CO<sub>2</sub> and CH<sub>4</sub> emissions vary with water table depth. *Nat. Clim. Chang.* 11 (9), 766–771. <https://doi.org/10.1038/s41558-021-01108-4>.
- Chiriboga, G., Bouillon, S., Borges, A.V., 2024. Dissolved greenhouse gas (CO<sub>2</sub>, CH<sub>4</sub>, N<sub>2</sub>O) emissions from highland lakes of the Andes cordillera in Northern Ecuador. *Aquat. Sci.* <https://doi.org/10.1007/s00027-023-01039-6>.
- Choudhury, M.I., McKie, B.G., Hallin, S., Ecke, F., 2018. Mixtures of macrophyte growth forms promote nitrogen cycling in wetlands. *Sci. Total Environ.* 635, 1436–1443. <https://doi.org/10.1016/j.scitotenv.2018.04.193>.
- Clifford, C.C., Heffernan, J.B., 2018. Artificial aquatic ecosystems. *Water* 10 (8), 1096. <https://doi.org/10.3390/w10081096>.
- Codispoti, L.A., Christensen, J.P., 1985. Nitrification, denitrification and nitrous oxide cycling in the eastern tropical South Pacific Ocean. *Mar. Chem.* 16 (4), 277–300. [https://doi.org/10.1016/0304-4203\(85\)90051-9](https://doi.org/10.1016/0304-4203(85)90051-9).
- Cole, J.J., Caraco, N.F., 2001. Carbon in catchments: connecting terrestrial carbon losses with aquatic metabolism. *Mar. Freshw. Res.* 52 (1), 101–110. <https://doi.org/10.1071/MF00084>.
- Cole, J.J., Caraco, N.F., 1998. Atmospheric exchange of carbon dioxide in a low-wind oligotrophic lake measured by the addition of SF<sub>6</sub>. *Limnol. Oceanogr.* 43 (4), 647–656. <https://doi.org/10.4319/lo.1998.43.4.0647>.
- Conrad, R., 2020. Methane production in soil environments—Anaerobic biogeochemistry and microbial life between flooding and desiccation. *Microorganisms* 8 (6), 881. <https://doi.org/10.3390/microorganisms8060881>.
- D’Acunha, B., Johnson, M.S., 2019. Water quality and greenhouse gas fluxes for stormwater detained in a constructed wetland. *J. Environ. Manage.* 231, 1232–1240. <https://doi.org/10.1016/j.jenvman.2018.10.106>.
- Dan, Z., Chuan, W., Qiaohong, Z., Xingzhong, Y., 2021. Sediments nitrogen cycling influenced by submerged macrophytes growing in winter. *Water Sci. Technol.* 83 (7), 1728–1738. <https://doi.org/10.2166/wst.2021.081>.
- Davidson, T.A., Audet, J., Svenning, J.C., Lauridsen, T.L., Søndergaard, M., Landkildehus, F., Jeppesen, E., 2015. Eutrophication effects on greenhouse gas fluxes from shallow-lake mesocosms override those of climate warming. *Glob. Chang. Biol.* 21 (12), 4449–4463. <https://doi.org/10.1111/gcb.13062>.
- Davidson, T.A., Sayer, C.D., Jeppesen, E., Søndergaard, M., Lauridsen, T.L., Johansson, L.S., Graeber, D., 2023. Bimodality and alternative equilibria do not help explain long-term patterns in shallow lake chlorophyll-a. *Nat. Commun.* 14 (1), 398. <https://doi.org/10.1038/s41467-023-36043-9>.
- De Backer, S., Van Onsem, S., Triest, L., 2010. Influence of submerged vegetation and fish abundance on water clarity in peri-urban eutrophic ponds. *Hydrobiologia* 656, 255–267. <https://doi.org/10.1007/s10750-010-0444-z>.
- Decina, S.M., Hutryra, L.R., Templer, P.H., 2020. Hotspots of nitrogen deposition in the world’s urban areas: a global data synthesis. *Front. Ecol. Environ.* 18 (2), 92–100. <https://doi.org/10.1002/fee.2143>.
- Del Giorgio, P.A., Cole, J.J., Caraco, N.F., Peters, R.H., 1999. Linking planktonic biomass and metabolism to net gas fluxes in northern temperate lakes. *Ecology* 80 (4), 1422–1431. [https://doi.org/10.1890/0012-9658\(1999\)080\[1422:LPBAMT\]2.0.CO;2](https://doi.org/10.1890/0012-9658(1999)080[1422:LPBAMT]2.0.CO;2).
- Del Giorgio, P.A., Peters, R.H., 1994. Patterns in planktonic P: R ratios in lakes: influence of lake trophy and dissolved organic carbon. *Limnol. Oceanogr.* 39 (4), 772–787. <https://doi.org/10.4319/lo.1994.39.4.0772>.
- DelSontro, T., Beaulieu, J.J., Downing, J.A., 2018. Greenhouse gas emissions from lakes and impoundments: upscaling in the face of global change. *Limnol. Oceanogr. Lett.* 3 (3), 64–75. <https://doi.org/10.1002/lo2.10073>.
- Descy, J.P., Leprieux, F., Pirlot, S., Leporcq, B., Van Wichelen, J., Peretyatko, A., Wilmotte, A., 2016. Identifying the factors determining blooms of cyanobacteria in a set of shallow lakes. *Ecol. Inform.* 34, 129–138. <https://doi.org/10.1016/j.ecoinf.2016.05.003>.
- Desrosiers, K., DelSontro, T., del Giorgio, P.A., 2022. Disproportionate contribution of vegetated habitats to the CH<sub>4</sub> and CO<sub>2</sub> budgets of a Boreal Lake. *Ecosystems* 1–20. <https://doi.org/10.1007/s10021-021-00730-9>.
- Dickson, A.G., Sabine, C.L., Christian, J.R., 2007. *Guide to Best Practices for Ocean CO<sub>2</sub> Measurement.* North Pacific Marine Science Organization, Sidney, British Columbia. <https://doi.org/10.25607/0BP-1342>, 191pp. (PICES Special Publication 3; IOCCP Report 8).
- Drake, T.W., Raymond, P.A., Spencer, R.G., 2018. Terrestrial carbon inputs to inland waters: a current synthesis of estimates and uncertainty. *Limnol. Oceanogr. Lett.* 3 (3), 132–142. <https://doi.org/10.1002/lo2.10055>.
- Duchemin, E., Lucotte, M., Canuel, R., 1999. Comparison of static chamber and thin boundary layer equation methods for measuring greenhouse gas emissions from large water bodies. *Environ. Sci. Technol.* 33 (2), 350–357. <https://doi.org/10.1021/es9800840>.
- Dutton, G., Elkins II, J., Hall, B., NOAA ESRL, 2017. *Earth System Research Laboratory Halocarbons and Other Atmospheric Trace Gases Chromatograph for Atmospheric Trace Species (CATS) Measurements.* NOAA National Centers for Environmental Information. <https://doi.org/10.7289/10.7289/NOAA0659V>. Version 1. [Database: atmospheric nitrous oxide N<sub>2</sub>O][2023-06-21].
- Erkkilä, K.M., Ojala, A., Bastviken, D., Biermann, T., Heiskanen, J.J., Lindroth, A., Mammarella, I., 2018. Methane and carbon dioxide fluxes over a lake: comparison between eddy covariance, floating chambers and boundary layer method. *Biogeosciences* 15 (2), 429–445. <https://doi.org/10.5194/bg-15-429-2018>.
- Gasith, A., Hosier, A.D., 1976. Airborne litterfall as a source of organic matter in lakes. *Limnol. Oceanogr.* 21 (2), 253–258. <https://doi.org/10.4319/lo.1976.21.2.0253>.
- Goreau, T.J., Kaplan, W.A., Wofsy, S.C., McElroy, M.B., Valois, F.W., Watson, S.W., 1980. Production of NO<sub>2</sub>- and N<sub>2</sub>O by nitrifying bacteria at reduced concentrations of oxygen. *Appl. Environ. Microbiol.* 40 (3), 526–532. <https://doi.org/10.1128/aem.40.3.526-532.1980>.
- Gorsky, A.L., Racanelli, G.A., Belvin, A.C., Chambers, R.M., 2019. Greenhouse gas flux from stormwater ponds in southeastern Virginia (USA). *Anthropocene* 28, 100218. <https://doi.org/10.1016/j.ancene.2019.100218>.
- Grasset, C., Abril, G., Mendonça, R., Roland, F., Sobek, S., 2019. The transformation of macrophyte-derived organic matter to methane relates to plant water and nutrient contents. *Limnol. Oceanogr.* 64 (4), 1737–1749. <https://doi.org/10.1002/lno.11148>.
- Grasset, C., Moras, S., Isidorova, A., Couture, R.M., Linkhorst, A., Sobek, S., 2021. An empirical model to predict methane production in inland water sediment from particular organic matter supply and reactivity. *Limnol. Oceanogr.* 66 (10), 3643–3655. <https://doi.org/10.1002/lno.11905>.
- Grasset, C., Sobek, S., Scharnweber, K., Moras, S., Villwock, H., Andersson, S., Hiller, C., Nydahl, A.C., Chaguaceda, F., Colom, W., Tranvik, L.J., 2020. The CO<sub>2</sub>-equivalent balance of freshwater ecosystems is non-linearly related to productivity. *Glob. Chang. Biol.* 26 (10), 5705–5715. <https://doi.org/10.1111/gcb.15284>.
- Grasshoff, K., Johannsen, H., 1972. A new sensitive and direct method for the automatic determination of ammonia in sea water. *ICES J. Mar. Sci.* 34 (3), 516–521. <https://doi.org/10.1093/icesjms/34.3.516>.
- Grasshoff, K., Kremling, K., Ehrhardt, M., 2009. *Methods of Seawater Analysis: Determination of Nitrite.* John Wiley & Sons.
- Grimham, A., Albert, S., Deering, N., Dunbabin, M., Bastviken, D., Sherman, B., Lovelock, C.E., Evans, C.D., 2018. The importance of small artificial water bodies as sources of methane emissions in Queensland, Australia. *Hydrol. Earth Syst. Sci.* 22 (10), 5281–5298. <https://doi.org/10.5194/hess-22-5281-2018>.
- Gruca-Rokosz, R., Cieślą, M., 2021. Sediment methane production within eutrophic reservoirs: the importance of sedimenting organic matter. *Sci. Total Environ.* 799, 149219 <https://doi.org/10.1016/j.scitotenv.2021.149219>.
- Guérin, F., Abril, G., Serça, D., Delon, C., Richard, S., Delmas, R., Tremblay, A., Varfalvy, L., 2007. Gas transfer velocities of CO<sub>2</sub> and CH<sub>4</sub> in a tropical reservoir and its river downstream. *J. Mar. Syst.* 66 (1–4), 161–172. <https://doi.org/10.1016/j.jmarsys.2006.03.019>.
- Hanson, P.C., Carpenter, S.R., Cardille, J.A., Coe, M.T., Winslow, L.A., 2007. Small lakes dominate a random sample of regional lake characteristics. *Freshw. Biol.* 52 (5), 814–822. <https://doi.org/10.1111/j.1365-2427.2007.01730.x>.
- Harpenslager, S.F., Thieme, K., Levertz, C., Misteli, B., Sebola, K.M., Schneider, S.C., Hilt, S., Köhler, J., 2022. Short-term effects of macrophyte removal on emission of CO<sub>2</sub> and CH<sub>4</sub> in shallow lakes. *Aquat. Bot.* 182, 103555 <https://doi.org/10.1016/j.aquabot.2022.103555>.
- Herrero Ortega, S., Romero González-Quijano, C., Casper, P., Singer, G.A., Gessner, M.O., 2019. Methane emissions from contrasting urban freshwaters: rates, drivers, and a whole-city footprint. *Glob. Chang. Biol.* 25 (12), 4234–4243. <https://doi.org/10.1111/gcb.14799>.
- Holgerson, M., Raymond, P., 2016. Large contribution to inland water CO<sub>2</sub> and CH<sub>4</sub> emissions from very small ponds. *Nat. Geosci.* 9, 222–226. <https://doi.org/10.1038/ngeo2654>.
- Holgerson, M.A., Farr, E.R., Raymond, P.A., 2017. Gas transfer velocities in small forested ponds. *J. Geophys. Res. Biogeosci.* 122 (5), 1011–1021. <https://doi.org/10.1002/2016JG003734>.
- IPCC: Intergovernmental Panel on Climate Change, 2019. *Refinement to the 2006 IPCC Guidelines For National Greenhouse Gas Inventories: Wetlands, 2019.* IPCC, Switzerland.
- Jansen, J., Thornton, B.F., Cortés, A., Snöälvi, J., Wik, M., MacIntyre, S., Crill, P.M., 2020. Drivers of diffusive CH<sub>4</sub> emissions from shallow subarctic lakes on daily to multi-year timescales. *Biogeosciences* 17 (7), 1911–1932. <https://doi.org/10.5194/bg-17-1911-2020>.
- Kankaala, P., Huotari, J., Tulonen, T., Ojala, A., 2013. Lake-size dependent physical forcing drives carbon dioxide and methane effluxes from lakes in a boreal landscape. *Limnol. Oceanogr.* 58 (6), 1915–1930. <https://doi.org/10.4319/lo.2013.58.6.1915>.
- Keller, M., Stallard, R.F., 1994. Methane emission by bubbling from Gatun Lake, Panama. *J. Geophys. Res.* 99 (D4), 8307–8319. <https://doi.org/10.1029/92JD02170>.

- Klaus, M., Vachon, D., 2020. Challenges of predicting gas transfer velocity from wind measurements over global lakes. *Aquat. Sci.* 82 (3), 53. <https://doi.org/10.1007/s00027-020-00729-9>.
- Koenker, R., 2005. *Quantile Regression*, 38. Cambridge university press. <https://doi.org/10.1017/CBO9780511754098>. Vol.
- Koroleff, J., 1983. Determination of total phosphorus by alkaline persulphate oxidation. *Methods of Seawater Analysis*. Verlag Chemie, Weinheim, pp. 136–138.
- Kortelainen, P., Larmola, T., Rantakari, M., Juutinen, S., Alm, J., Martikainen, P.J., 2020. Lakes as nitrous oxide sources in the boreal landscape. *Glob. Chang. Biol.* 26 (3), 1432–1445. <https://doi.org/10.1111/gcb.14928>.
- Lapierre, J.F., del Giorgio, P.A., 2012. Geographical and environmental drivers of regional differences in the lake pCO<sub>2</sub> versus DOC relationship across northern landscapes. *J. Geophys. Res. Biogeosci.* (G3), 117. <https://doi.org/10.1029/2012JG001945>.
- ... & Lauerwald, R., Regnier, P., Figueiredo, V., Enrich-Prast, A., Bastviken, D., Lehner, B., Raymond, P., 2019. Natural lakes are a minor global source of N<sub>2</sub>O to the atmosphere. *Glob. Biogeochem. Cycles* 33 (12), 1564–1581. <https://doi.org/10.1029/2019GB006261>.
- Liao, R., Miao, Y., Li, J., Li, Yan, Wang, Z., Du, J., Li, Yueming, Li, A., Shen, H., 2018. Temperature dependence of denitrification microbial communities and functional genes in an expanded granular sludge bed reactor treating nitrate-rich wastewater. *RSC Adv.* 8 (73), 42087–42094. <https://doi.org/10.1039/c8ra08256a>.
- Lorke, A., Bodmer, P., Noss, C., Alshboul, Z., Koschorreck, M., Somlai-Haase, C., Bastviken, D., Flury, S., McGinnis, D.F., Maeck, A., Müller, D., Premke, K., 2015. Drifting versus anchored flux chambers for measuring greenhouse gas emissions from running waters. *Biogeosciences* 12 (23), 7013–7024. <https://doi.org/10.5194/bg-12-7013-2015>.
- Maberly, S.C., Barker, P.A., Stott, A.W., De Ville, M.M., 2013. Catchment productivity controls CO<sub>2</sub> emissions from lakes. *Nat. Clim. Chang.* 3 (4), 391–394. <https://doi.org/10.1038/nclimate1748>.
- ... & Mander, Ü., Tournebize, J., Espenberg, M., Chaumont, C., Torga, R., Garnier, J., Soosaar, K., 2021. High denitrification potential but low nitrous oxide emission in a constructed wetland treating nitrate-polluted agricultural run-off. *Sci. Total Environ.* 779, 146614. <https://doi.org/10.1016/j.scitotenv.2021.146614>.
- Martinez-Cruz, K., Gonzalez-Valencia, R., Sepulveda-Jauregui, A., Plascencia-Hernandez, F., Belmonte-Izquierdo, Y., Thalasso, F., 2017. Methane emission from aquatic ecosystems of Mexico City. *Aquat. Sci.* 79, 159–169. <https://doi.org/10.1007/s00027-016-0487-y>.
- McClure, R.P., Lofton, M.E., Chen, S., Krueger, K.M., Little, J.C., Carey, C.C., 2020. The magnitude and drivers of methane ebullition and diffusion vary on a longitudinal gradient in a small freshwater reservoir. *J. Geophys. Res. Biogeosci.* 125 (3) <https://doi.org/10.1029/2019JG005205>.
- McCrackin, M.L., Elser, J.J., 2011. Greenhouse gas dynamics in lakes receiving atmospheric nitrogen deposition. *Glob. Biogeochem. Cycles* 25 (4). <https://doi.org/10.1029/2010GB003897>.
- Mehring, A.S., Kuehn, K.A., Tant, C.J., Pringle, C.M., Lowrance, R.R., Vellidis, G., 2014. Contribution of surface leaf-litter breakdown and forest composition to benthic oxygen demand and ecosystem respiration in a South Georgia blackwater river. *Freshw. Sci.* 33 (2), 377–389. <https://doi.org/10.1086/675507>.
- Mengis, M., Gächter, R., Wehrli, B., 1997. Sources and sinks of nitrous oxide (N<sub>2</sub>O) in deep lakes. *Biogeochemistry* 38, 281–301. <https://doi.org/10.1023/A:1005814020322>.
- Myrhe, G., Shindell, D., Bréon, F.M., Collins, W., Al, E., 2013. Anthropogenic and natural radiative forcing. *Climate Change 2013 The Physical Science Basis: working Group I Contribution to the Fifth Assessment Report of the Intergovernmental Panel on Climate Change. Chapter 8 : Anthropogenic and Natural Radiative Forcing* 9781107057, 659–740. [doi:10.1017/CBO9781107415324.018](https://doi.org/10.1017/CBO9781107415324.018).
- Myrstener, M., Jonsson, A., Bergström, A.K., 2016. The effects of temperature and resource availability on denitrification and relative N<sub>2</sub>O production in boreal lake sediments. *J. Environ. Sci.* 47, 82–90. <https://doi.org/10.1016/j.jes.2016.03.003>.
- Natchimuthu, S., Panneer Selvam, B., Bastviken, D., 2014. Influence of weather variables on methane and carbon dioxide flux from a shallow pond. *Biogeochemistry* 119, 403–413. <https://doi.org/10.1007/s10533-014-9976-z>.
- Ni, B.J., Rusalleda, M., Pellicer-Nacher, C., Smets, B.F., 2011. Modeling nitrous oxide production during biological nitrogen removal via nitrification and denitrification: extensions to the general ASM models. *Environ. Sci. Technol.* 45 (18), 7768–7776. <https://doi.org/10.1021/es404125v>.
- Ni, M., Liang, X., Hou, L., Li, W., He, C., 2022. Submerged macrophytes regulate diurnal nitrous oxide emissions from a shallow eutrophic lake: a case study of Lake Wuliangshui in the temperate arid region of China. *Sci. Total Environ.* 811, 152451. <https://doi.org/10.1016/j.scitotenv.2021.152451>.
- Nijman, T.P., Lemmens, M., Lurling, M., Kosten, S., Welte, C., Veraart, A.J., 2022. Phosphorus control and dredging decrease methane emissions from shallow lakes. *Sci. Total Environ.* 847, 157584. <https://doi.org/10.1016/j.scitotenv.2022.157584>.
- Oksanen, R.J., Simpson, G.L., Blanchet, F.G., Solyomos, P., Stevens, M.H.H., Szocs, E., Wagner, H., Barbour, M., Bedward, M., Bolker, B., Borcard, D., Carvalho, G., Chirico, M., Durand, S., Beatriz, H., Evangelista, A., Friendly, M., Hannigan, G., Hill, M.O., Lahti, L., Mcglinn, D., Ribeiro, E., Smith, T., Stier, A., Ter, C.J.F., Weedon, J., (2013). Package 'vegan'. *Community ecology package, version*, 2(9), 1–295. <https://cran.r-project.org/web/packages/vegan/index.html>.
- Olid, C., Rodellas, V., Rocher-Ros, G., Garcia-Orellana, J., Diego-Feliu, M., Alorda-Kleinglass, A., Bastviken, D., Karlsson, J., 2022. Groundwater discharge as a driver of methane emissions from Arctic lakes. *Nat. Commun.* 13, 3667. <https://doi.org/10.1038/s41467-022-31219-1>.
- Ollivier, Q.R., Maher, D.T., Pitfield, C., Macreadie, P.I., 2019. Punching above their weight: large release of greenhouse gases from small agricultural dams. *Glob. Chang. Biol.* 25 (2), 721–732. <https://doi.org/10.1111/gcb.14477>.
- Palacin-Lizarbe, C., Camarero, L., Catalan, J., 2018. Denitrification temperature dependence in remote, cold, and N-Poor Lake sediments. *Water Resour. Res.* 54 (2), 1161–1173. <https://doi.org/10.1002/2017WR021680>.
- Pataki, D.E., Carreiro, M.M., Cherrier, J., Grulke, N.E., Jennings, V., Pincetl, S., Pouyat, R.V., Whitlow, T.H., Zipperer, W.C., 2011. Coupling biogeochemical cycles in urban environments: ecosystem services, green solutions, and misconceptions. *Front. Ecol. Environ.* 9 (1), 27–36. <https://doi.org/10.1890/090220>.
- Peacock, M., Audet, J., Bastviken, D., Cook, S., Evans, C.D., Grinham, A., Holgerson, M.A., Högbom, L., Pickard, A.E., Zieliński, P., Futter, M.N., 2021. Small artificial waterbodies are widespread and persistent emitters of methane and carbon dioxide. *Glob. Chang. Biol.* 27 (20), 5109–5123. <https://doi.org/10.1111/gcb.15762>.
- Peacock, M., Audet, J., Jordan, S., Smeds, J., Wallin, M.B., 2019. Greenhouse gas emissions from urban ponds are driven by nutrient status and hydrology. *Ecosphere* 10 (3), e02643. <https://doi.org/10.1002/ecs2.2643>.
- Peretyatko, A., Symoens, J.J., Triest, L., 2007. Impact of macrophytes on phytoplankton in eutrophic peri-urban ponds, implications for pond management and restoration. *Belg. J. Bot.* 83–99. <https://www.jstor.org/stable/20794626>.
- Peretyatko, A., Teissier, S., De Backer, S., Triest, L., 2012. Classification trees as a tool for predicting cyanobacterial blooms. *Hydrobiologia* 689, 131–146. <https://doi.org/10.1007/s10750-011-0803-4>.
- Peretyatko, A., Teissier, S., De Backer, S., Triest, L., 2010. Restoration potential of biomanipulation for eutrophic peri-urban ponds: the role of zooplankton size and submerged macrophyte cover. *Pond Conserv. Eur.* 281–291. <https://doi.org/10.1007/s10750-009-9888-4>.
- Perolo, P., Fernández Castro, B., Escoffier, N., Lambert, T., Bouffard, D., Perga, M.E., 2021. Accounting for surface waves improves gas flux estimation at high wind speed in a large lake. *Earth Syst. Dyn.* 12 (4), 1169–1189. <https://doi.org/10.5194/esd-12-1169-2021>.
- R Core Team, 2022. R: a language and environment for statistical computing. <https://www.r-project.org/>.
- Rabaey, J., Cotner, J., 2022. Pond greenhouse gas emissions controlled by duckweed coverage. *Front. Environ. Sci.* 10, 889289. <https://doi.org/10.3389/fenvs.2022.889289>.
- Ray, N.E., Holgerson, M.A., Andersen, M.R., Bortolotti, L.E., Futter, M., Kokor, I., Law, A., McDonald, C., Mesman, J.P., Peacock, M., 2023. Spatial and temporal variability in summertime dissolved carbon dioxide and methane in temperate ponds and shallow lakes. *Limnol. Oceanogr.* <https://doi.org/10.1002/lno.12362>.
- Raymond, P.A., Hartmann, J., Lauerwald, R., Sobek, S., McDonald, C., Hoover, M., Butman, D., Striegl, R., Mayorga, E., Humborg, C., Kortelainen, P., Dürr, H., Meybeck, M., Ciais, P., Guth, P., 2013. Global carbon dioxide emissions from inland waters. *Nature* 503 (7476), 355–359. <https://doi.org/10.1038/nature12760>.
- Rosamond, M.S., Thuss, S.J., Schiff, S.L., 2012. Dependence of riverine nitrous oxide emissions on dissolved oxygen levels. *Nat. Geosci.* 5 (10), 715–718. <https://doi.org/10.1038/ngeo1556>.
- Rosentreter, J.A., Borges, A.V., Deemer, B.R., Holgerson, M.A., Liu, S., Song, C., Melack, J., Raymond, P.A., Duarte, C.M., Allen, G.H., Olefeldt, D., Poulter, B., Battin, T.L., Eyre, B.D., 2021. Half of global methane emissions come from highly variable aquatic ecosystem sources. *Nat. Geosci.* 14 (4), 225–230. <https://doi.org/10.1038/s41561-021-00715-2>.
- Sand-Jensen, K., Staehr, P.A., 2007. Scaling of pelagic metabolism to size, trophy and forest cover in small Danish lakes. *Ecosystems* 10, 128–142. <https://doi.org/10.1007/s10021-006-9001-z>.
- Singh, S.N., Kulshreshtha, K., Agnihotri, S., 2000. Seasonal dynamics of methane emission from wetlands. *Chemosphere Glob. Chang. Sci.* 2 (1), 39–46. [https://doi.org/10.1016/S1465-9972\(99\)00046-X](https://doi.org/10.1016/S1465-9972(99)00046-X).
- Sønderup, M.J., Egemose, S., Hansen, A.S., Grudinina, A., Madsen, M.H., Flindt, M.R., 2016. Factors affecting retention of nutrients and organic matter in stormwater ponds. *Ecology* 9 (5), 796–806. <https://doi.org/10.1002/eco.1683>.
- Soued, C., Del Giorgio, P.A., Maranger, R., 2016. Nitrous oxide sinks and emissions in boreal aquatic networks in Québec. *Nat. Geosci.* 9 (2), 116–120. <https://doi.org/10.1038/ngeo2611>.
- U.S. EPA. 2007. "Method 3015A (SW-846): microwave assisted acid digestion of aqueous samples and extracts," Revision 1. Washington, DC <https://www.epa.gov/esam/epa-method-3015a-microwave-assisted-acid-digestion-aqueous-samples-and-extracts>.
- U.S. EPA. 1994. "Method 200.7: determination of metals and trace elements in water and wastes by inductively coupled plasma-atomic emission spectrometry," Revision 4.4. Cincinnati, OH. <https://www.epa.gov/esam/method-2007-determination-metals-and-d-trace-elements-water-and-wastes-inductively-coupled>.
- van Bergen, T.J.H.M., Barros, N., Mendonça, R., Aben, R.C.H., Althuisen, I.H.J., Huszar, V., Lamers, L.P.M., Lüring, M., Roland, F., Kosten, S., 2019. Seasonal and diel variation in greenhouse gas emissions from an urban pond and its major drivers. *Limnol. Oceanogr.* 64 (5), 2129–2139. <https://doi.org/10.1002/lno.11173>.
- van Nes, E.H., Scheffer, M., van den Berg, M.S., Coops, H., 2002. Dominance of charophytes in eutrophic shallow lakes—when should we expect it to be an alternative stable state? *Aquat. Bot.* 72 (3–4), 275–296. [https://doi.org/10.1016/S0304-3770\(01\)00206-6](https://doi.org/10.1016/S0304-3770(01)00206-6).
- Velthuis, M., Veraart, A.J., 2022. Temperature sensitivity of freshwater denitrification and N<sub>2</sub>O emission—a meta-analysis. *Glob. Biogeochem. Cycles* 36 (6). <https://doi.org/10.1029/2022GB007339> e2022GB007339.
- Vingiani, F., Durighetto, N., Klaus, M., Schelker, J., Labasque, T., Botter, G., 2021. Evaluating stream CO<sub>2</sub> outgassing via drifting and anchored flux chambers in a

- controlled flume experiment. *Biogeosciences* 18 (3), 1223–1240. <https://doi.org/10.5194/bg-18-1223-2021>.
- Wanninkhof, R., 1992. Relationship between gas exchange and wind speed over the ocean. *J. Geophys. Res.* 97, 7373–7381. <https://doi.org/10.1029/92JC00188>.
- Webb, J.R., Leavitt, P.R., Simpson, G.L., Baulch, H.M., Haig, H.A., Hodder, K.R., Finlay, K., 2019. Regulation of carbon dioxide and methane in small agricultural reservoirs: optimizing potential for greenhouse gas uptake. *Biogeosciences* 16 (21), 4211–4227. <https://doi.org/10.5194/bg-16-4211-2019>.
- Wetzel, R.G., 2001. *Limnology: Lake and River Ecosystems*. Gulf Professional Publishing.
- Weyhenmeyer, G.A., Kosten, S., Wallin, M.B., Tranvik, L.J., Jeppesen, E., Roland, F., 2015. Significant fraction of CO<sub>2</sub> emissions from boreal lakes derived from hydrologic inorganic carbon inputs. *Nat. Geosci.* 8 (12), 933–936. <https://doi.org/10.1038/ngeo2582>.
- Yentsch, C.S., Menzel, D.W., 1963. A method for the determination of phytoplankton chlorophyll and phaeophytin by fluorescence. In: *Deep Sea Research and Oceanographic Abstracts*, 10. Elsevier, pp. 221–231. [https://doi.org/10.1016/0011-7471\(63\)90358-9](https://doi.org/10.1016/0011-7471(63)90358-9).
- Yvon-Durocher, G., Allen, A.P., Bastviken, D., Conrad, R., Gudas, C., St-Pierre, A., Thanh-Duc, N., Del Giorgio, P.A., 2014. Methane fluxes show consistent temperature dependence across microbial to ecosystem scales. *Nature* 507 (7493), 488–491. <https://doi.org/10.1038/nature13164>.
- Zeikus, J.G., Winfrey, M., 1976. Temperature limitation of methanogenesis in aquatic sediments. *Appl. Environ. Microbiol.* 31 (1), 99–107. <https://doi.org/10.1128/aem.31.1.99-107.1976>.